COPY 1
PM
85/11

DOT/FAA/PM-85/11

Program Engineering
and Maintenance Service
Washington, D.C. 20591

Automatic Detection of Gust Fronts

AVAILABLE IN
ELECTRONIC FORMAT

Hiroshi Uyeda
Dusan S. Zrnic'

National Severe Storms Laboratory
1313 Halley Circle
Norman, Oklahoma 73069

FEDERAL AVIATION ADMINISTRATION

JUL 2 1985

TECHNICAL CENTER LIBRARY
ATLANTIC CITY, N.J. 08405

April 1985

Final Report

This document is available to the public through the National Technical Information Service, Springfield, Virginia 22161.

U.S. Department of Transportation
Federal Aviation Administration

NOTICE

This document is disseminated under the sponsorship of the Department of Transportation in the interest of information exchange. The United States Government assumes no liability for its contents or use thereof.

Technical Report Documentation Page

1. Report No. DOT/FAA/PM-85/11	2. Government Accession No.	3. Recipient's Catalog No.
4. Title and Subtitle Automatic Detection of Gust Fronts		5. Report Date April 1985
		6. Performing Organization Code MGG000
7. Author(s) Hiroshi Uyeda and Dusan S. Zrnic'		8. Performing Organization Report No.
9. Performing Organization Name and Address National Severe Storms Laboratory 1313 Halley Circle Norman, OK 73069		10. Work Unit No. (TRAIS)
		11. Contract or Grant No. DTFA01-80-Y-10524
12. Sponsoring Agency Name and Address U.S. Department of Transportation Federal Aviation Administration Systems Engineering & Maintenance Service Washington, D.C. 20591		13. Type of Report and Period Covered Subtask A Final Report
		14. Sponsoring Agency Code APM-310

15. Supplementary Notes

16. Abstract

We have developed a procedure that detects and tracks gust fronts automatically. It does not rely on a single method but requires simultaneous operation of two related algorithms. The convergence algorithm measures radial convergence and hence only gusts propagating along radials can be readily detected. The mesocyclone-shear algorithm measures azimuthal shear and is suitable for detecting gusts parallel with radials as well as low level vortices. Long shear lines that these algorithms detect are classified as gusts whereas symmetric shear features are rejected if their shear and momentum are insignificant; otherwise they are classified as low level vortices. To track gusts we use second order polynomials in the range-azimuth plane. It is shown that predicted gust locations from simple linear projections of the least square fitted curves agree very well with actual gust locations.

17. Key Words Gust Fronts Automatic Tracking Algorithm NEXRAD		18. Distribution Statement Document is available to the U.S. public through the National Technical Information Service, Springfield, Virginia 22151.	
19. Security Classif. (of this report) Unclassified	20. Security Classif. (of this page) Unclassified	21. No. of Pages 66	22. Price

Form DOT F 1700.7 (8-72) Reproduction of completed page authorized

PREFACE

We appreciate the help of Yosefa Gal-Chen during the initial stages of algorithm development. Don Burgess provided us with the information concerning the weather situation on April 26, 1984, when TWA flight 163 encountered turbulence. Lindsay Murdock contributed editorial changes, Joy Walton and Michelle Foster typed the manuscript and Joan Kimpel and Bob Goldsmith produced the figures. Part of this work was supported by the Joint Systems Program Office of NEXRAD.

TABLE OF CONTENTS

List of Figures

List of Tables

1. Introduction.....1

2. Gust Front Characteristics.....1

3. Pattern Recognition Algorithm.....5

3.1 Detection of Radial Convergence.....5

3.2 Velocity Dealiasing.....10

3.3 Construction of Pattern Vectors.....11

3.4 Gradient and "Flux" Thresholds.....15

3.5 Detection of Azimuthal Shear.....20

3.6 Tracking of Gust Fronts.....21

4. Case Studies.....24

4.1 April 13, 1981.....24

4.2 May 9, 1981.....33

4.3 May 29, 1980.....33

4.4 April 10, 1981.....38

4.5 April 26, 1984.....43

5. Summary and Conclusions.....44

References.....49

LIST OF FIGURES

Figure 1a. Gust front of April 26, 1984. Velocity color categories in $m \cdot s^{-1}$ are indicated on the right. Reds represent velocities away from the radar; dark blue indicates regions where echoes are overlaid in range.

Figure 1b. Spectrum width; color categories at right are in $m \cdot s^{-1}$.

Figure 1c. Effective reflectivity factor in dBZ. Range marks are 40 km apart, and the cursor indicates the location of Will Rogers airport.

Figure 2. Flow chart of pattern recognition algorithm.

Figure 3. (a) Doppler velocities along a radial showing aliasing that cannot be corrected with a simple continuity check. The unambiguous velocity $v_a = 25.6\ m \cdot s^{-1}$.
(b) The same velocities dealiased. The gust front convergence region extends from about 18 km to 27 km.

Figure 4. The logic of dealiasing. The three straight lines indicate possible relationships between input (aliased) and output (dealiased) velocities. As long as the dealiased velocities along a radial are on a single line, convergence measurements will be correct.

Figure 5. The procedure for the construction of pattern vectors. Dots represent the boundaries of segments that are joined by the algorithm.

Figure 6a. Profiles of equivalent reflectivity factor, mean velocity and Doppler spectrum width along radials for a gust of April 13, 1981. Both raw and nine-point averaged mean velocities are shown. The spectrum width is a nine-point running average. The beginning, B, and ending, E, of the pattern vectors are indicated.

Figure 6b. Profiles as in Fig. 6a, for the gust of May 9, 1981.

Figure 6c. Profiles as in Fig. 6b; the radial is now tangent to the frontal discontinuity. The arrow indicates a subjectively deduced location of the front from the spatial continuity of the mean velocities (see Fig. 1).

Figure 7. Two features of pattern vectors identified by the algorithm for May 9, 1981. The azimuthally elongated feature at 40 km is a genuine gust front.

Figure 8a. Profiles as in Fig.6a, at a different azimuth. Beginning and ending of each pattern vector are indicated; g is gradient and f is "flux".

Figure 8b. Four features of pattern vectors identified by the algorithm for April 13, 1981. The first and second features are produced by the primary and secondary surges.

Figure 9. Detection region for pattern vectors in the gradient - "flux" plane. Data are for the April 13, 1981, portion of the front extending over 10° in azimuth that was (a) perpendicular to the radials and (b) almost parallel to the radials.

Figure 10. Detection region for pattern vectors in the gradient - "flux" plane. Data are for the May 9, 1981, portion of the front extending over 10° in azimuth that was (a) perpendicular to the radials and (b) almost parallel to the radials.

Figure 11. Twisting downburst of May 30, 1982. The center of this downburst is at -80 km, 18 km from the Norman radar. Wind vectors were obtained from data of two Doppler radars, and the scale vector is indicated in the lower left corner. This downburst is imbedded in strong reflectivities as seen from the extent of the 50 dBZ contour. The leading edge of the outflow NE of the center (thick line) would exhibit anticyclonic shear to any radar located north or south of it. Parallel to this line and about 3 km west of it the radars would detect a cyclonic shear. (Courtesy Mike Eilts, NSSL).

Figure 12. Detection region for the pattern vectors in the shear momentum plane applicable to the mesocyclone shear algorithm. Data are for the indicated portion (azimuth, range) of the front of April 10, 1981.

Figure 13. Doppler velocities for the gust front of April 13, 1981. Elevation is 1.3°, range marks are 20 km apart, and red represents velocities away from the radar. Patches of red in the middle of green are aliased velocities, most likely due to outflow produced by intense downdrafts.

Figure 14. Contours of mean Doppler velocities for the gust front of April 13, 1981. The contour interval is 10 $m \cdot s^{-1}$. Objectively determined location of the front (thick line) is superposed. The square next to C is at the center (r_c, az_c) of the front.

Figure 15. Detected gusts at an elevation of 0.8° for the front of April 13, 1981. The locations of maximum gradients and their five-point running averages are plotted. Superposed also are the least squares fitted lines. The primary gust is labeled with 1 and the secondary surge with 2.

Figure 16a. Detected gust lines at a constant elevation of 1.3° at three consecutive times. The lines are five-point running averages of maximum gradient locations. Numbers 1, 2, and 3 identify features with time continuity.

Figure 16b. Detected gust lines in one volume scan Numbers 1, 2, and 3 correspond to the same features as in Fig. 16a, which are continuous through four heights

Figure 17a. Three consecutive positions of the front (April 13, 1981). The smooth curves are least squares fits to the data and the forecast position is indicated. The range mark is at 40 km from the radar. Centers of the pattern vectors were used to trace the gust. Squares indicate the centers of these three front lines.

Figure 17b. Consecutive positions of the front, as in Fig.17a except that locations of maximum gradients were used to trace the gust.

Figure 18a. RMS error between the fitted curve (primary gust) and (1) center of pattern vectors and (2) locations of maximum gradients. Data are from three consecutive times (ranges) for April 13, 1981. The range is to the centers of features, which differ slightly for the two methods.

Figure 18b. Full circles are RMS errors as in Fig. 18a, plotted versus height. Open circles are RMS errors for the gust front at other than 1.2-1.3° in elevation, these are not plotted on Fig. 18a.

Figure 19a. Area, average "flux", average gradient, and average of maximum gradients versus range for the gust of April 13, 1981.

Figure 19b. Parameters as in Fig.19a, plotted versus height.

Figure 20a. Detected gust fronts. Dashed line is a five-point running average of maximum gradient locations (from convergence algorithm, same as "1" on Fig. 16a) and the solid line is a five-point running average of pattern vector centers (from mesocyclone-shear algorithm).

Figure 20b. Actual positions of the gust and a forecast position obtained from the mesocyclone-shear algorithm.

Figure 21. Doppler velocities for the gust front of May 9, 1981. Range marks are 40 km apart, elevation is 1°, and the cursor is near the center of the front.

Figure 22. Contours of mean Doppler velocities for the gust front of May 9, 1981. The contour interval is 10 $m \cdot s^{-1}$. Objectively determined location of the front (thick line) is superposed.

Figure 23. Detected gust lines at a constant elevation of 1°. The curves labeled "1" are part of the same gust. Locations of maximum gradients, their five-point averages, and least squares fitted positions are plotted.

Figure 24. Three consecutive positions of the front on May 9, 1981. The smooth curves are least square fits to data, and the forecast position is indicated.

Figure 25. RMS error between the fitted curve and gust positions determined by the location of maximum gradients for May 9, 1981.

Figure 26. Area, average "flux", average gradient, and average of maximum gradient versus range for the gust of May 9, 1981.

Figure 27. Doppler velocity display for the gust front of May 29, 1980. Range marks are 40 km apart, elevation is 0.9°, and the cursor is near a low-level vortex.

Figure 28a. Contours of mean Doppler velocities of the gust front of May 29, 1980. The contour interval is 10 $m \cdot s^{-1}$. Objectively determined location of the front (thick line) is superposed. The small circle indicates the core of a mesocyclonic vortex, and the dashed circle has a diameter three times larger than the core.

Figure 28b. Three consecutive positions of the front on May 29, 1980. The smooth curves are least squares fits to the data, and the forecast position is indicated. The range mark is at 40 km from the radar.

Figure 29. Area, average "flux", and average gradient versus range for the gust of May 29, 1980.

Figure 30. Display of mean velocities for the gust front of April 10, 1981. Range marks are 40 km apart, elevation is 0.8°, and the cursor locates the front. The area NW of the white square is contaminated with second-trip echoes.

Figure 31a. Shear lines detected by the mesocyclone-shear algorithm at 2300 CST on April 10, 1981, at 0.8° elevation. The data, their five-point average and the least squares fitted curves are drawn.

Figure 31b. Shear lines as in Fig.31a, at 2306 CST.

Figure 31c. Shear lines as in Fig. 31b, at 1.2° elevation.

Figure 32a. Shear lines detected by the gradient algorithm for April 26, 1984. The data, their five-point average, and the least square fitted curves are drawn.

Figure 32b. Three consecutive positions of the front. Five-point running average, least squares fitted curves, and a forecast position are shown. Square indicates the center of each curve.

Figure 33. Algorithm for detecting weather hazards near the ground.

LIST OF TABLES

Table 1 Thresholds for Detecting Radial Convergence Lines

Table 2 Thresholds for Detecting Azimuthal Shear Lines

Table 3 Parameters for the April 13, 1981, Front

Table 4 Parameters for the May 9, 1981, Front

Table 5 Parameters for the May 29, 1981, Front

Table 6 Parameters for the April 10, 1981, Front

Table 7 Parameters for the April 26, 1984, Front

Table 8 Average Parameters for Five Gust Fronts

AUTOMATIC DETECTION OF GUST FRONTS

Hiroshi Uyeda and Dusan S. Zrnic'

1. Introduction

Early displays of Doppler spectral moments demonstrated that many hazardous weather features produce characteristic signatures that human observers can readily interpret (Wood and Brown 1983). Among the most dramatic signatures are those of mesocyclonic circulations (Sirmans and Doviak 1973); tornado vortex signatures (Brown **et al.,** 1978); divergence signatures (Zrnic' and Gal-Chen 1983; Doviak and Zrnic', 1984; Wilson **et al.,** 1984); and shear lines associated with gust fronts (Zrnic' and Lee, 1983). Although recognition of these signatures by trained human observers is not complicated, there are strong reasons to develop automated techniques that would help or in some cases even replace the human operator It is well known that humans excel machines by far in recognizing patterns. Yet when several patterns need to be examined, quantified, and remembered for correlations in space or time, the machines become superior. Furthermore, a machine's performance is consistent regardless of the environmental conditions and is not subject to the boredom and fatigue that affect humans. With procurement plans for Next Generation Weather Radar (NEXRAD) well under way, a need exists to provide as much assistance as possible to interpretation of radar displays. So far, several algorithms have been developed and tested to serve that purpose (NEXRAD Algorithm Report, 1984). This paper concerns algorithms that detect and track gust fronts. Our procedure is based on gradients of radial velocity. These are grouped by features, whose shapes are examined.

2. Gust Front Characteristics

An intense gust front propagating toward or away from the radar produces at low levels a very well defined line of convergent radial velocities (Fig. 1a). The frontal position is also detectable from the Doppler spectrum

widths, which are large (Fig. 1b) at the front, behind it, and in this case ahead of it. Alas, the reflectivity field offers almost no clue to the precise position of the front (Fig. 1c) and none whatever about the turbulence ahead. A TWA flight 163 encountered severe turbulence on approach to the Will Rogers Airport (cursor on the figure) at the time the data in Fig. 1 were recorded. The approach had to be aborted, and the flight was diverted to Tulsa. Because real-time Doppler information was not available, subsequent flights also had to be diverted to Tulsa or Lubbock for safety reasons.

The reflectivity display (color scale in dBZ) indicates a line of heavy thunderstorms whose leading edge is about 10 km northwest of the tower. The line is moving to the east, and individual cells are moving to the northeast. Maximum reflectivity values near the ground are in excess of 55 dBZ; reflectivities aloft exceed 60 dBZ. Radar reflectivity at low levels

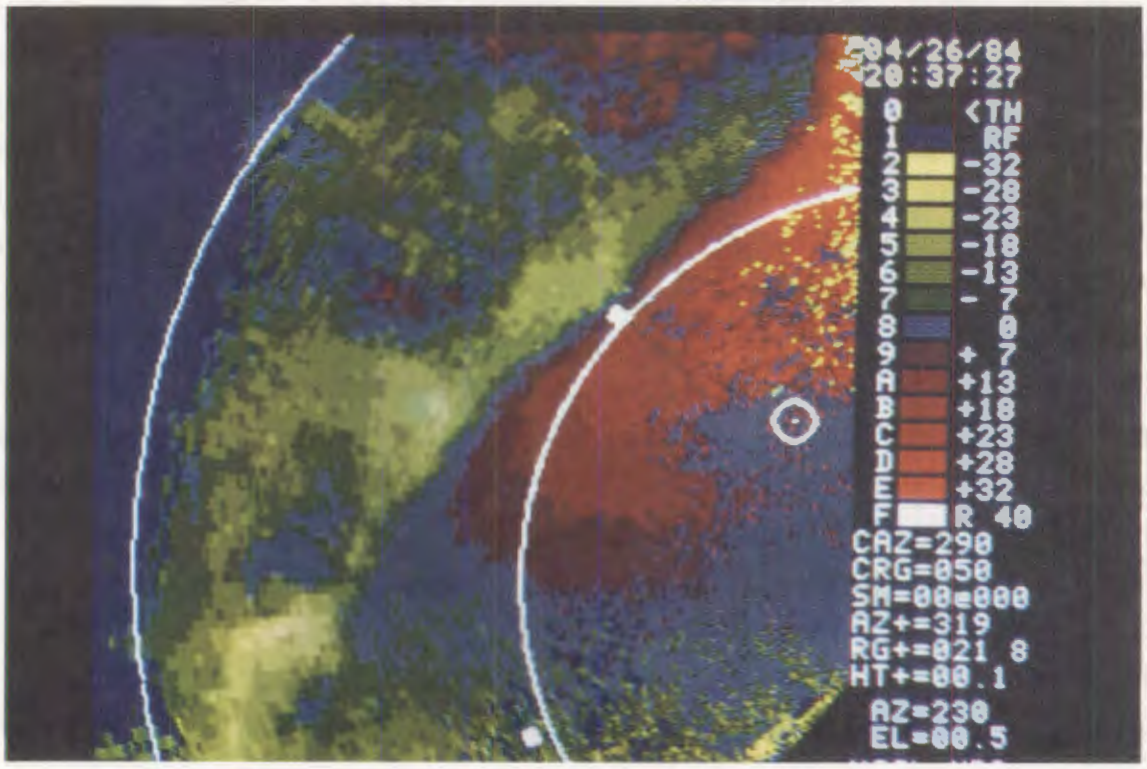

Figure 1(a) Gust front of April 26, 1984. Velocity color categories in m·s^{-1} are indicated on the right. Reds represent velocities away from the radar; dark blue indicates regions where echoes are overlaid in range.

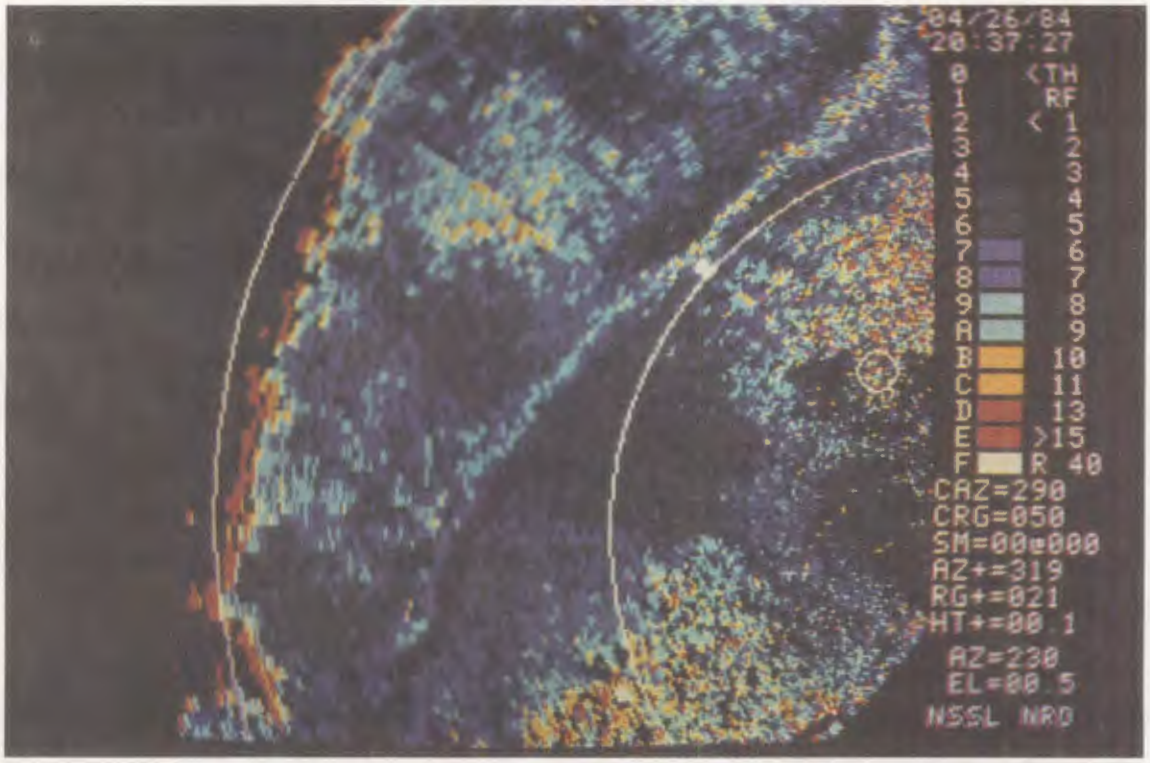

Figure 1(b) Spectrum width; color categories at right are in $m \cdot s^{-1}$.

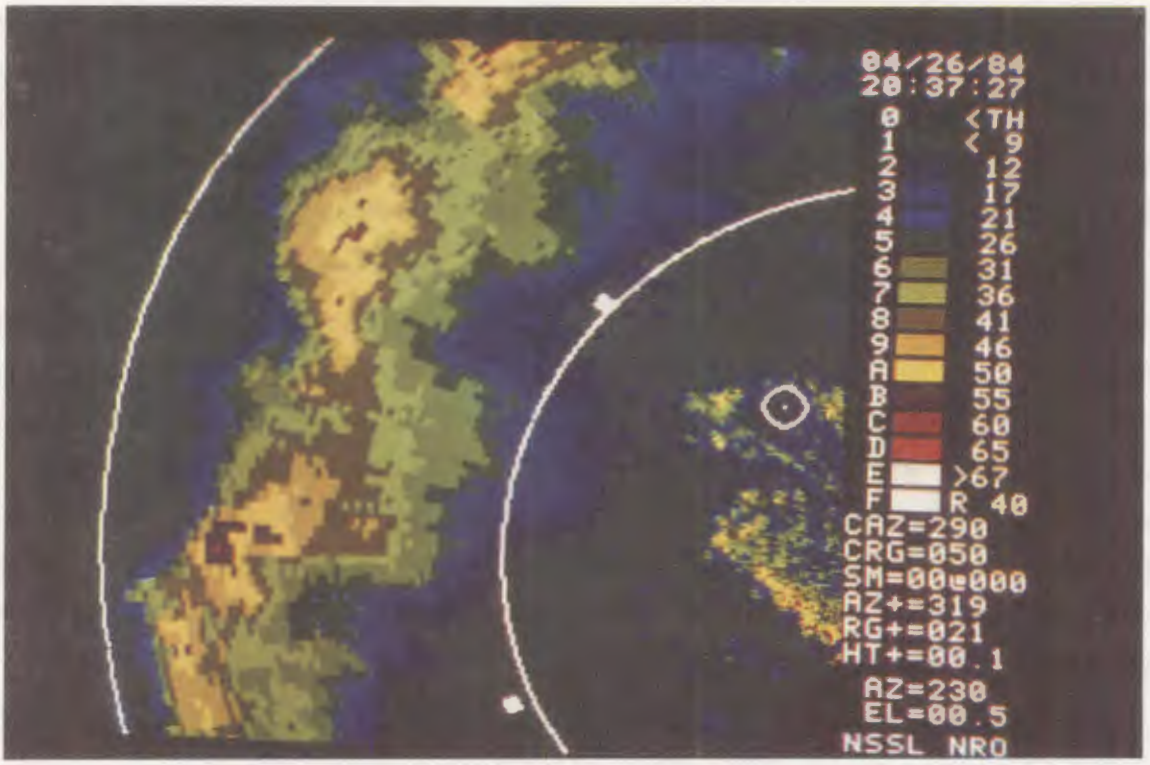

Figure 1(c) Effective reflectivity factor in dBZ. Range marks are 40 km apart, and the cursor indicates the location of Will Rogers airport.

ahead of the front is weak (less than 9 dBZ) and probably does not result from raindrops, but instead from refractive index gradients of the air and discrete particles caught up in the wind.

The velocity display color code (at right) shows radial flow components toward the radar as green to yellow and away from the radar as red to orange values are in meters per second (multiply by 2 for approximate value in knots). In regions where the real velocity exceeds the maximum unambiguous velocity measurable by the radar ($\pm$ 34 $m \cdot s^{-1}$), the velocity aliases on the color scale. Strong outbound flow is displayed as bright red up to 34 $m \cdot s^{-1}$ but as bright yellow to green when it exceeds 34 $m \cdot s^{-1}$. Such a pattern is visible to the north of Norman where bright red surrounds many small areas of bright yellow. Blue is reserved for regions where velocity parameters cannot be estimated because of overlay of echoes.

A meteorological feature prominent on the velocity display is a convergence boundary or gust front extending from north at 80 km to west at 40 km. The strong southerly winds ahead of the gust front (bright red and yellow) apparently identify a low-level jet associated with the storm system. The rapid changes from red to yellow reveal that the flow is not constant but posesses strong shears. These features are verified from wind measurements recorded on the KTVY tower. Strong south winds are gusting up to 25 $m \cdot s^{-1}$ at the surface and gusting higher than 35 $m \cdot s^{-1}$ at the topmost level (444 m or 1500 ft). Velocity data at other elevation angles confirm that the strong flow extends up to the aircraft altitude (6000 ft) and beyond.

The spectrum width is a measure of the spread of velocity about the mean velocity at each sample location. Large widths are produced by strong wind shears and turbulence. The display shows extremely turbulent flow in bright blue, yellow, and red (widths greater than 8 $m \cdot s^{-1}$). Note that the display indicates large widths ahead of the tower. This is confirmed by high variability in the recorded tower winds, which change by as much as 14 $m \cdot s^{-1}$ in 10 seconds. The gust front position shows up as a narrow zone of large widths to the west and north of the tower by a few kilometers (same region as that shown on the velocity display).

The aircraft may have encountered severe turbulence in a low-level jet ahead of the gust front. The meteorological explanation for the extreme turbulence of the low-level jet is not obvious. The frequency of occurrence

of such flows as hazards to aircraft is not well known either. On the other hand, the aircraft may have crossed the gust line; its altitude was such that it would not have penetrated the gravity current but would have been in the turbulent storm inflow just above it.

Characteristics like the ones on Fig. 1 have been documented for several fronts (Zrnic' and Lee, 1983), and a detailed discussion of their dynamics in the lower 400 m can be found in the report by Goff (1975). It was observed that the lengths of these fronts were from 12 to 90 km. On the basis of these observations and our previous experience with the divergence algorithm (Zrnic' and Gal-Chen, 1983), we decided to attempt detection of the convergence line in the Doppler velocity field. Thus, we have applied the principles from the divergence algorithm, to detect convergence lines instead. The convergence occurs about the frontal discontinuity because fluids with two different velocities are moving toward each other. The cool outflow air is flowing underneath the warm moist inflow. Ahead of the outflow the environmental air has a strong velocity component toward the front. For most orientations of the gust front except when it is parallel to a radial, a Doppler radar would detect convergence as a decrease in the velocities along a radial. Our algorithm capitalizes on this simple fact. However, fronts parallel to radials do not produce radial convergence signatures. To detect such fronts the mesocyclone-shear detection algorithm must be used. We show, by means of two examples, how and with what thresholds the mesocyclone-shear algorithm works in detecting low-level azimuthal shear.

3. Pattern Recognition Algorithm

3.1 Detection of Radial Convergence

Our gust front pattern recognition algorithm is modeled after the mesocyclone and divergence algorithms (Zrnic' et al., 1984; Zrnic' and Gal-Chen, 1983). Therefore only a brief description is given here. The algorithm starts by searching along a radial for runs of decreasing velocities, which characterize radial convergence. This search is done by comparing consecutive velocities. When a run terminates, a pattern vector is formed; its six components are beginning velocity v_b, ending velocity v_e, beginning range r_b, ending range r_e, azimuth, and maximum gradient g_m defined by

$$g_m = \max \left(\frac{v_{n-4} - v_{n+4}}{r_{n+4} - r_{n-4}}\right) \tag{1}$$

where v_n is a smoothed (i.e., nine-point average) velocity corresponding to a range r_n between beginning and ending ranges of a pattern vector. We estimate this gradient from data spaced nine points apart because (see Section 3.2) the spacing further smoothes the gradient over the same (matched) length as the one used for averaging the velocities.

Before the pattern vector is saved for further processing, its gradient defined as

$$g = \frac{v_b - v_e}{r_e - r_b} \tag{2}$$

and "flux"

$$f = (v_b - v_e)\ (r_e - r_b) \tag{3}$$

are checked against a set of thresholds (Fig. 2). If the vector fails low gradient L_g or low "flux" L_f thresholds, it is discarded; otherwise, a check against high thresholds is made. If the vector passes either high "flux" H_f or high gradient H_g thresholds, it is saved for later sorting. We caution the reader that the term "flux" used here is a carry-over from the divergence algorithm. It has physical meaning only if the flow in a plane has a point source or sink with significant influence over a circle with diameter $r_e - r_b$. In addition to the already listed thresholds, data are processed only if reflectivities are larger than -15 dBZ and heights are less than 2 km. All the thresholds and their values used in the present study are summarized in Table 1.

After the completion of a scan, all saved pattern vectors are sorted into features according to their proximity. Two vectors belong to the same feature if the range and azimuth centers r_{ci}, az_{ci} satisfy

$$(|r_{ci} - r_{cj}| < \ell_r) \text{ and } (|az_i - az_j| < \ell_a) \tag{4}$$

where ℓ_r is a threshold for radial distance and ℓ_a for azimuthal distance.

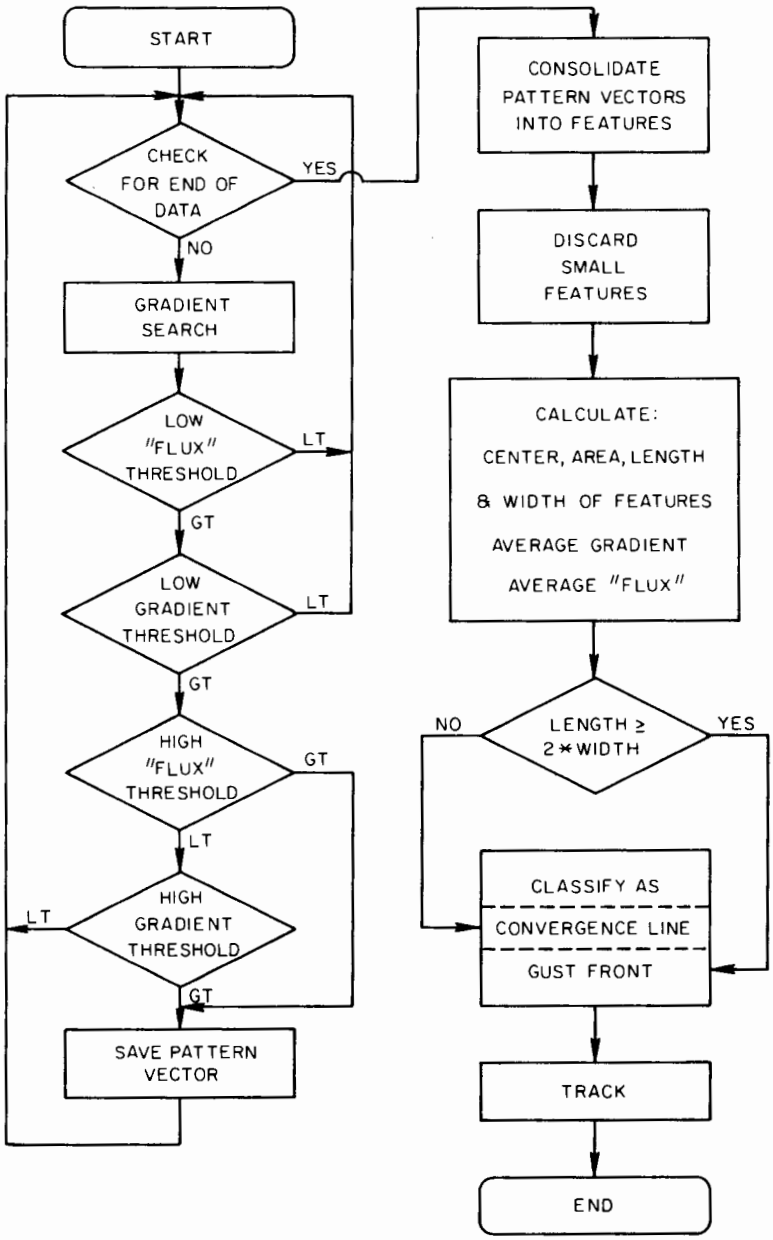

Figure 2 Flow chart of pattern recognition algorithm.

Features with very few pattern vectors are immediately discarded; the remaining features are further processed. For each feature the algorithm computes the following:

Azimuth center

$$az_c = \frac{1}{M} \Sigma\, az_i \tag{5}$$

Range center

$$r_c = \frac{1}{2M} \Sigma (r_b + r_e)_i \tag{6}$$

Average radial convergence

$$CONV = \frac{1}{M} \Sigma \left(\frac{v_b - v_e}{r_e - r_b}\right)_i \tag{7}$$

Maximum radial convergence

$$MAXCONV = \max \left(\frac{v_b - v_e}{r_e - r_b}\right)_i \tag{8}$$

Average of the maximum gradient

$$G = \frac{1}{M} \Sigma g_{mi} \tag{9}$$

Average velocity difference

$$DELV = \frac{1}{M} \Sigma (v_e - v_b)_i \tag{10}$$

Maximum velocity difference

$$MAXDELV = \max (v_e - v_b)_i \tag{11}$$

Average "flux"

$$F = \frac{1}{M} \Sigma [(v_b - v_e) (r_e - r_b)]_i \tag{12}$$

Maximum "flux"

$$MAXF = \max [(v_b - v_e) (r_e - r_b)]_i \tag{13}$$

Area

$$A = \frac{\pi}{720} \Sigma (az_{i+1} - az_i) (r_b + r_e)_i [(r_e - r_b)_i + (r_e - r_b)_{i+1}] \tag{14}$$

Length

$$L = \Sigma \{[\frac{\pi}{360} (az_{i+1}-az_i) (r_b+r_e)_i]^2 + [(r_b+r_e)_{i+1} - (r_b+r_e)_i]^2/4\}^{1/2} \quad (15)$$

Average width

$$W = \frac{1}{M} \Sigma (r_e - r_b)_i \quad (16)$$

where M is the number of pattern vectors in a feature.

TABLE 1

Thresholds for Detecting Radial Convergence Lines

THRESHOLD	NUMERICAL VALUE
High Gradient	$H_g = 0.65\ m \cdot s^{-1} \cdot km^{-1}$
Low Gradient	$L_g = 0.50\ m \cdot s^{-1} \cdot km^{-1}$
High "Flux"	$H_f = 100\ m \cdot s^{-1} \cdot km$
Low "Flux"	$L_f = 30\ m \cdot s^{-1} \cdot km$
Max. azimuthal separation between vectors	$\ell_a = 4°$
Max. range separation between vectors	$\ell_r = 4.0$ km
Reflectivity Threshold	-15 dBZ
Height Threshold	2 km (and below)

Features with azimuthal length L, larger by a factor of 2 from average width W, are classified as fronts (F). Features with smaller azimuthal lengths are classified as shear lines (S). We have often observed that pattern vectors representing secondary surges are classified in the same feature as the primary gust front. This is because pattern vectors are statistical and our distance criterion is liberal. Therefore pattern vectors in a feature that lie on the same radial (i.e., have the same azimuths) are

separated. So if the gust front is approaching the radar, all pattern vectors along common radials with centers farthest from the radar are taken out of the feature and classified as belonging to a secondary surge. Contrary to this when the front is receding, pattern vectors along common radials that are closer to the radar are classified in a secondary surge feature.

3.2 Velocity Dealiasing

Dealiasing of velocities is not an inherent part of the algorithm. Nevertheless, we found it necessary to dealias the velocities. When intense gust fronts are propagating toward the radar, there are many regions where the velocities exceed their unambiguous interval, 2 v_a. In order for this or any other algorithm to perform properly, the input velocities must be valid. Our first attempt at dealiasing consisted of checking the continuity of radial velocities and making corrections whenever a difference between two consecutive velocities exceeded the unambiguous value v_a. This procedure works well whenever the discontinuity is an abrupt step. However, we have often found that the discontinuity is less abrupt. For example, in Fig. 3a the discontinuity at 25 km extends over three consecutive range bins and is such that the difference between any two consecutive velocities is less than v_a. Consequently, the simple continuity check fails. Rather than build an extensive continuity check with look-ahead capability, we compared a nine-point running average with the first nonaveraged value outside the nine points. The choice of a nine-point running average is an expedient one because we are using a nine-point average for gradient measurements anyway (see Section 3.3). When the velocities are 150 m apart, the nine-point average extends over 1.35 km, which is less than the width of the convergence zone in the gust front. For the analyzed gust fronts our dealiasing procedure has performed well so far. As seen in Fig. 3b, all velocities are correctly dealiased except the one near zero, which can be considered an outlier. Outliers can be easily eliminated by checking the spread of velocities about the running average. We do not check for outliers because our procedure to build pattern vectors is immune to bursts of outliers that span less than six consecutive values (see Section 3.3).

Measurement of convergence is sensitive only to the difference of velocities and therefore is not affected when all the velocities along a radial are dealiased consistently though wrongly. This is illustrated in Fig. 4.

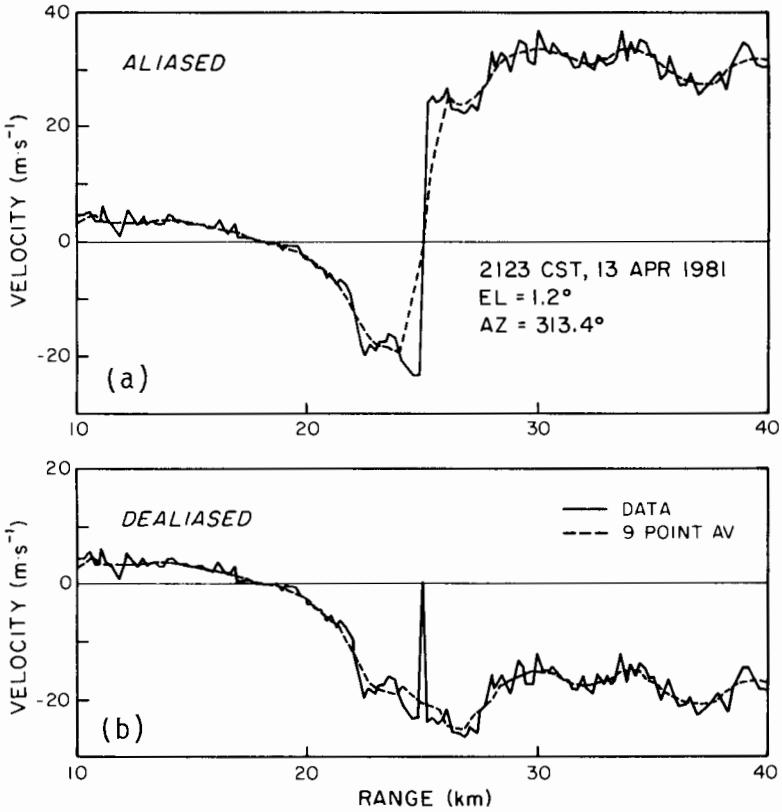

Figure 3 (a) Doppler velocities along a radial showing aliasing that cannot be corrected with a simple continuity check. The unambiguous velocity $v_a = 25.6\ m \cdot s^{-1}$. (b) The same velocities dealiased. The gust front convergence region extends from about 18 km to 27 km.

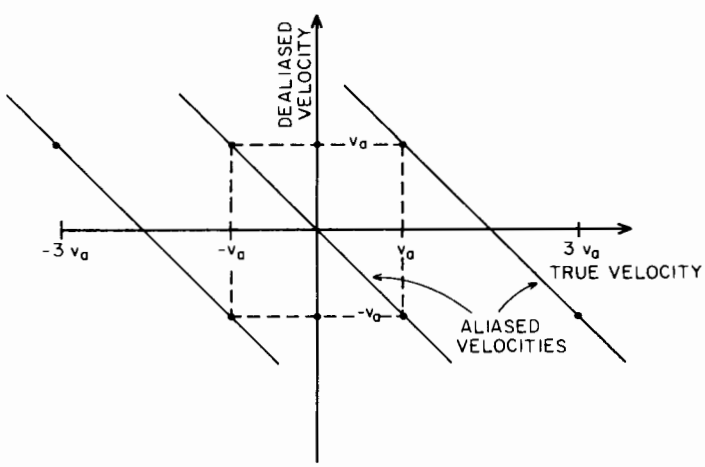

Figure 4 The logic of dealiasing. The three straight lines indicate possible relationships between input (aliased) and output (dealiased) velocities. As long as the dealiased velocities along a radial are on a single line, convergence measurements will be correct.

3.3 Construction of Pattern Vectors

The method by which pattern vectors are obtained in the gust front algorithm is somewhat different from that used in the mesocyclone algorithm. Namely, a nine-point running average of the velocities along a radial is first performed so that the effective range resolution is 1.35 km. This equals the

minimum width of a 2-dBZ gust contour (Zrnic' and Lee, 1983). Averaging reduces the fluctuations due to estimation errors and turbulence. But even with this smoothing, we observed that deviations of velocities about a linear fit in range were enough to break up what seems to be a single, continuous pattern vector.

We contrast these results with those of mesocyclone algorithm where comparisons of adjacent velocities are sufficient to yield valid pattern vectors. The reason for the difference is twofold: (1) Resolution volume weighting function in the azimuthal direction is broader than in the range direction, and the overlap is more from one azimuth to the next than from one range location to the next. Therefore, the increase of velocities through the mesocyclone core is more likely to be monotonic with azimuth than the decrease of the velocities through a gust with range. (2) Range locations are only 150 m apart whereas adjacent azimuthal distances are of the order of a kilometer. Therefore, for equal shear the percent deviation of incremental velocity (due to noise) with respect to the mean between two adjacent range locations is considerably larger than the corresponding percent deviation between two adjacent azimuths.

For these reasons we have added a seven-point look ahead capability to our vector construction routine. The procedure looks at seven adjacent (in range) velocities and selects the maximum of the minima, which is less than or equal to the current velocity. Thus, the algorithm leaps from a maximin location to a next maximin point and connects the segments until there is an increase (over more than seven consecutive points) of velocities with range. This principle is illustrated in Fig. 5 where dots indicate boundaries between segments that the algorithm has connected.

In the tested examples, our procedure has provided very good performance, but the computing time for pattern vector generation is larger than in the mesocyclone algorithm. We believe that increased computational speed would be possible without sacrificing accuracy if coarser range resolution were used.

Next we show several examples of Doppler spectral moments along radials that are cutting through gust fronts (Figs. 6a, b) or are tangential to the front (Fig. 6c). An increase in reflectivity is evident for the two cases shown in Figs. 6a and 6b where the radials are perpendicular to the fronts. However, these increases are not displaced by the same amount from the

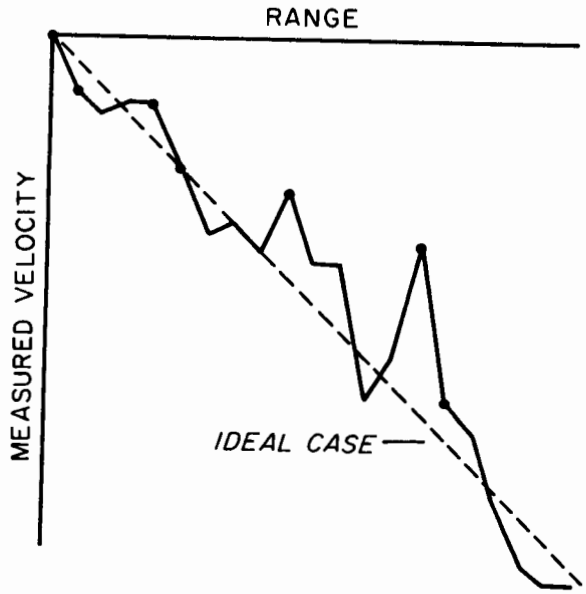

Figure 5 The procedure for the construction of pattern vectors. Dots represent the boundaries of segments that are joined by the algorithm.

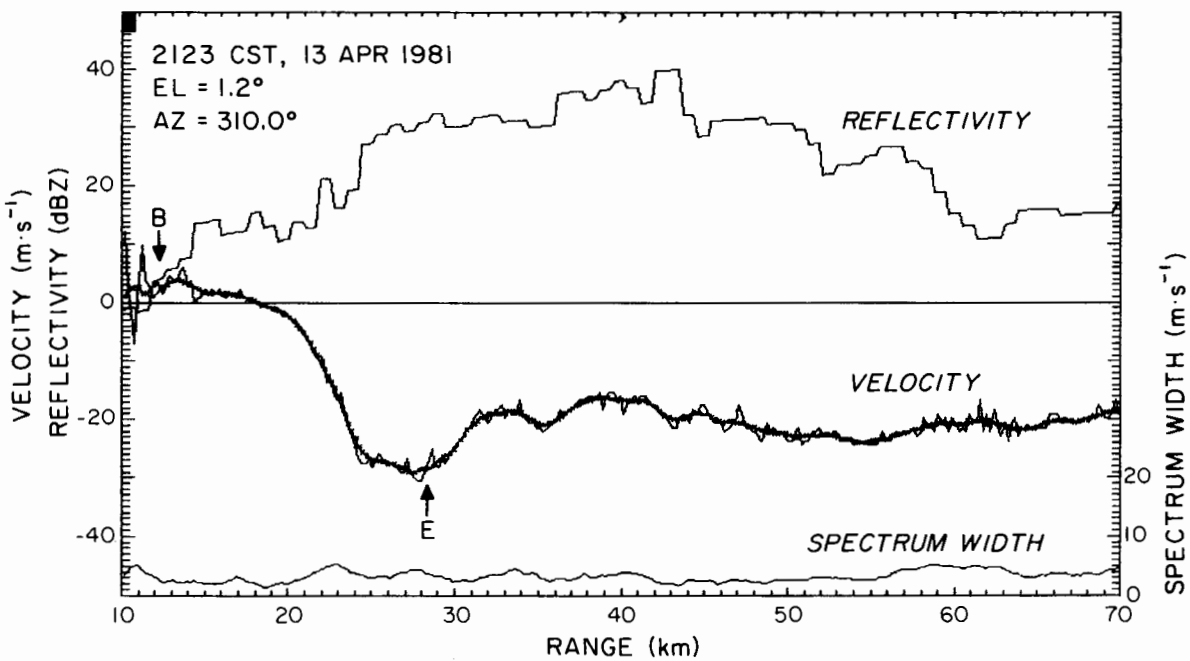

Figure 6(a) Profiles of equivalent reflectivity factor, mean velocity and Doppler spectrum width along radials for a gust of April 13, 1981. Both raw and nine-point averaged mean velocities are shown. The spectrum width is a nine-point running average. The beginning, B, and ending, E, of the pattern vectors are indicated.

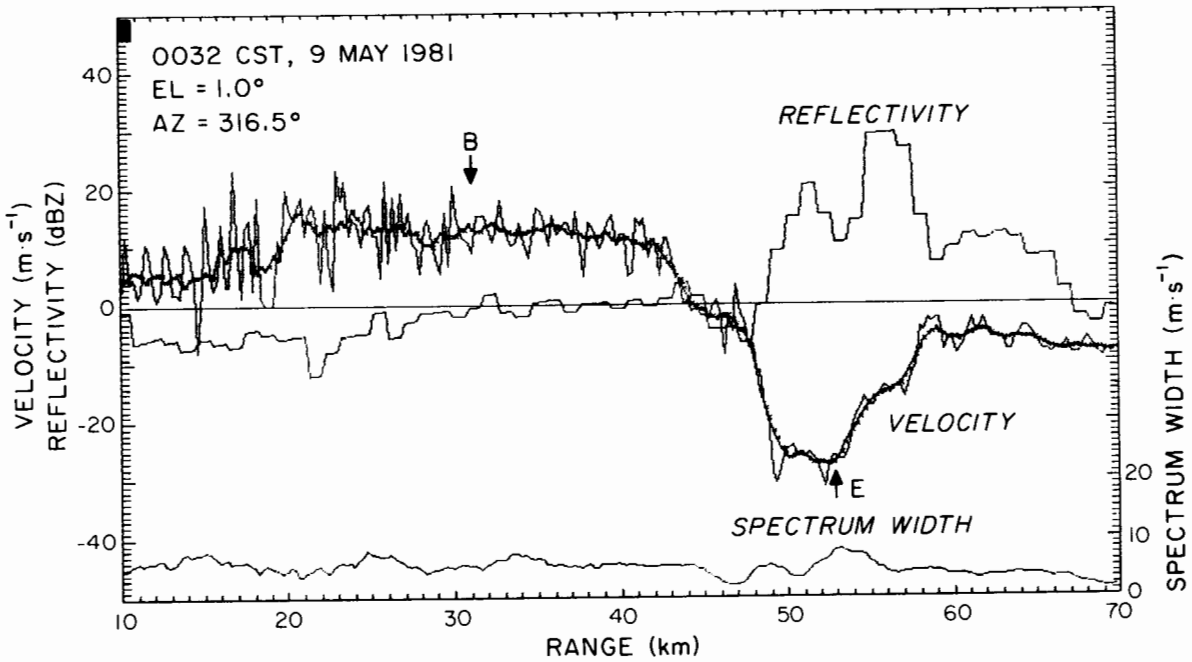

Figure 6(b) Profiles as in Fig. 6a, for the gust of May 9, 1981.

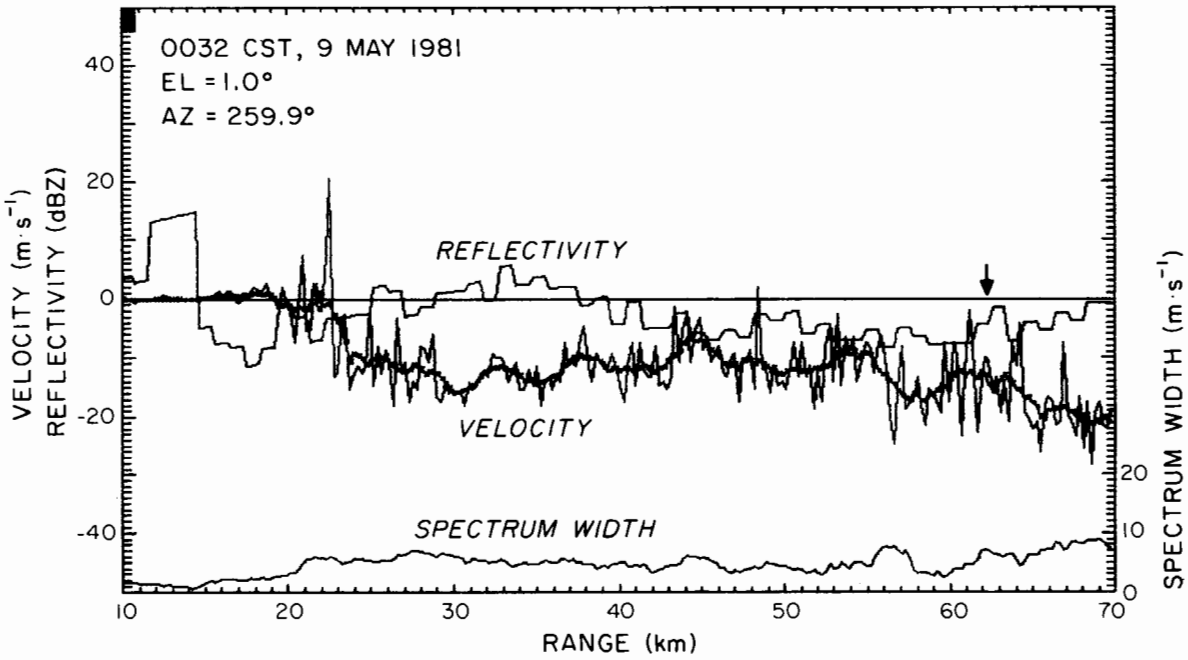

Figure 6(c) Profiles as in Fig. 6b; the radial is now tangent to the frontal discontinuity. The arrow indicates a subjectively deduced location of the front from the spatial continuity of the mean velocities (see Fig. 1).

location of maximum gradients. For the gust of April 13 the reflectivity increases about 10 km ahead of the maximum velocity gradient whereas on May 9 the increase coincides with the maximum gradient of velocities. Note that when the radial is tangent to the front (Fig. 6c), no clear signatures are obtainable from the spectral moments along a radial. Otherwise the smoothed mean velocities clearly exhibit a region of large gradient, which is included in pattern vectors whose beginnings and endings are indicated in Figs. 6a and 6b. It is apparent in these figures that the location of maximum gradient is a better indicator of the front's position than the midpoint of the pattern vector (see Section 4.1). From the plot of Doppler spectrum width we cannot easily locate the fronts although slight local maxima coincide with the maximum gradients.

Pattern vectors for the scan at 1° in elevation (May 9, 1981) were classified into two features (Fig. 7). The closer feature is spurious and has resulted from ground clutter contaminations. The velocities at the beginning of pattern vectors (i.e., closest to the radar) are not representative of the environmental flow but are heavily biased toward zero by echoes from the ground. Farther away at the pattern vectors' end, the velocities are more representative of the environmental flow with a component toward the radar. Hence, artificial gradients are created, but because its length to width ratio is less than 2, the feature is not classified as a gust front. The azimuthally elongated feature at 40 km is correctly classified as a gust front.

Often behind the front there are secondary surges (Goff, 1975) and convergence regions produced by small downdrafts. In Fig. 8a the primary (B_1-E_1) and secondary (B_2-E_2) gusts have about equal maximum gradients whereas the other three convergences are characterized by maximum gradients at least five times lower. Only the pattern vectors (B_1-E_1), (B_2-E_2), and (B_3-E_3) pass the first screening thresholds and are saved for later sorting into features. The feature to which (B_3-E_3) belongs is not long enough and hence is discarded, and only two gust features are identified at this elevation (Fig. 8b).

3.4 Gradient and "Flux" Thresholds

Because our detection algorithm relies heavily on kinematic properties of gust fronts (i.e., gradient and "flux"), we present here some statistical data concerning these quantities that influenced the choices in Table 1. We had

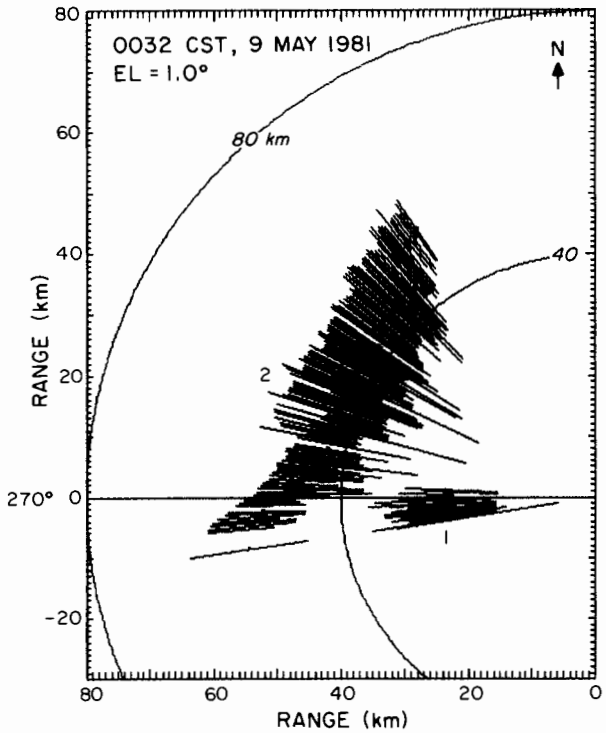

Figure 7 Two features of pattern vectors identified by the algorithm for May 9, 1981. The azimuthally elongated feature at 40 km is a genuine gust front.

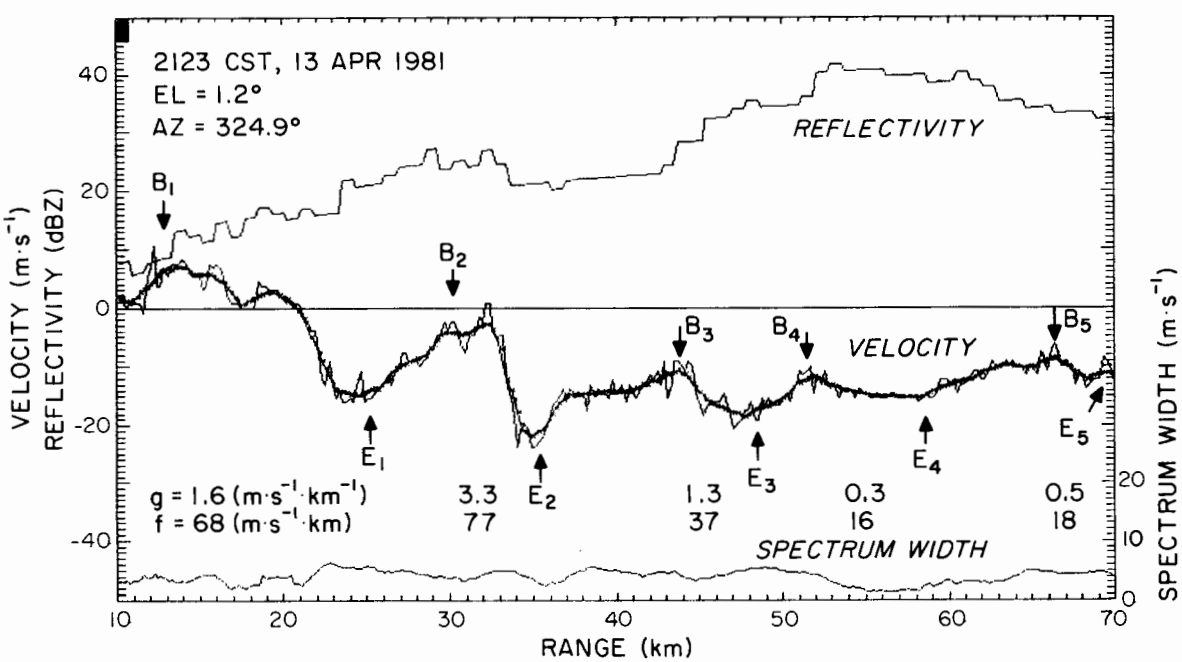

Figure 8(a) Profiles as in Fig.6a, at a different azimuth. Beginning and ending of each pattern vector are indicated; g is gradient and f is "flux".

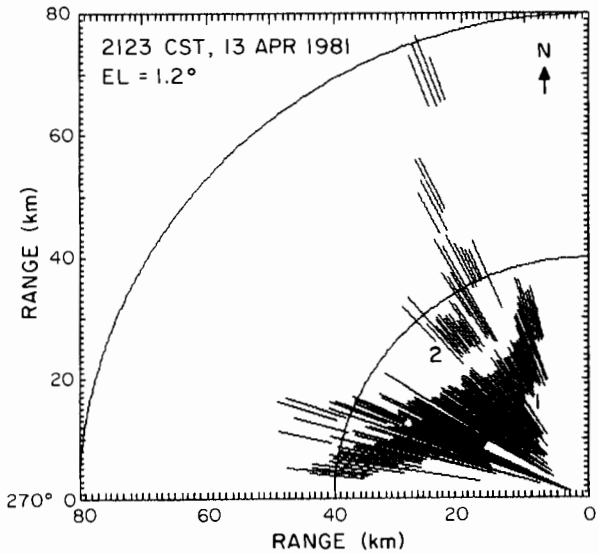

Figure 8(b) Four features of pattern vectors identified by the algorithm for April 13, 1981. The first and second features are produced by the primary and secondary surges.

examined the gradient versus "flux" data for two gust fronts in order to obtain the detection region in the gradient - "flux" plane on Figs. 9 and 10. This region is also described by the thresholds in Table 1. The gradient "flux" points on Fig. 9a for pattern vectors belonging to a gust front of April 13, 1981, are well separated from the points belonging to other convergence regions because the front is perpendicular to the radials. When the front is almost tangential, the separation between pattern vectors is not as striking (Fig. 9b), yet in this example, there is little overlap. For the gust front of May 9, 1981, we see again (Fig. 10a) that the separation is excellent when angles between the radial and the front are nearly perpendicular. In the other extreme, where the front is almost along the radials, the separation is poor and the chosen thresholds (Fig. 10b) are optimized to distinguish between pattern vectors belonging to the gust and the ones from convergence zones. From Figs. 9 and 10 it is evident that detection is not very sensitive to small variation of thresholds about the chosen values; a 20 percent variation in one of the thresholds would result in a couple of missed pattern vectors or in a couple of false pattern vectors. Since the detection algorithm sorts pattern vectors according to proximity with rather conservative distances (Table 1), we note that a loss of several vectors does not affect detection. Similarly, false vectors are extremely unlikely to form elongated features and thus are rejected by the sorting routine. Therefore, we expect our thresholds to work well for a variety of gusts having orientations similar to the radar beam as was the case for

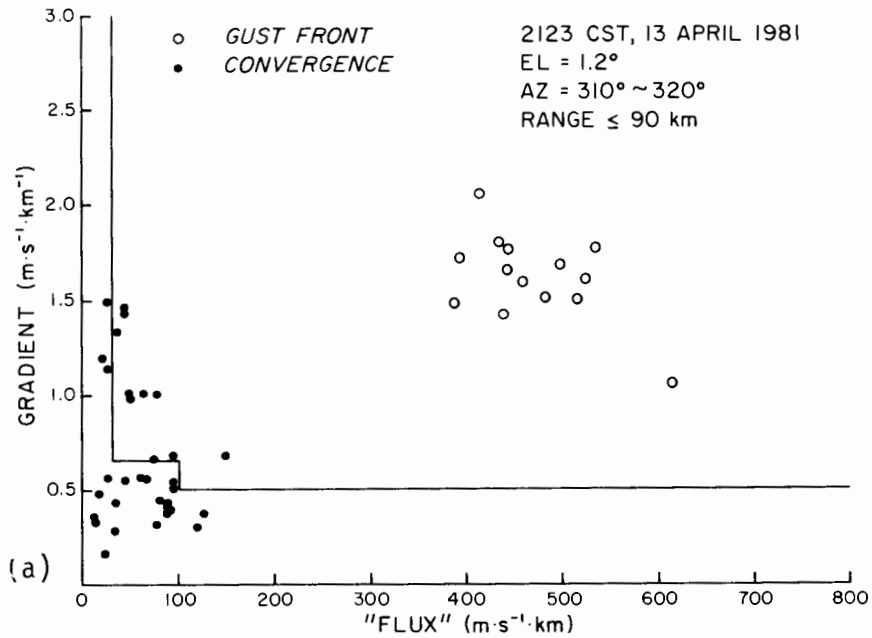

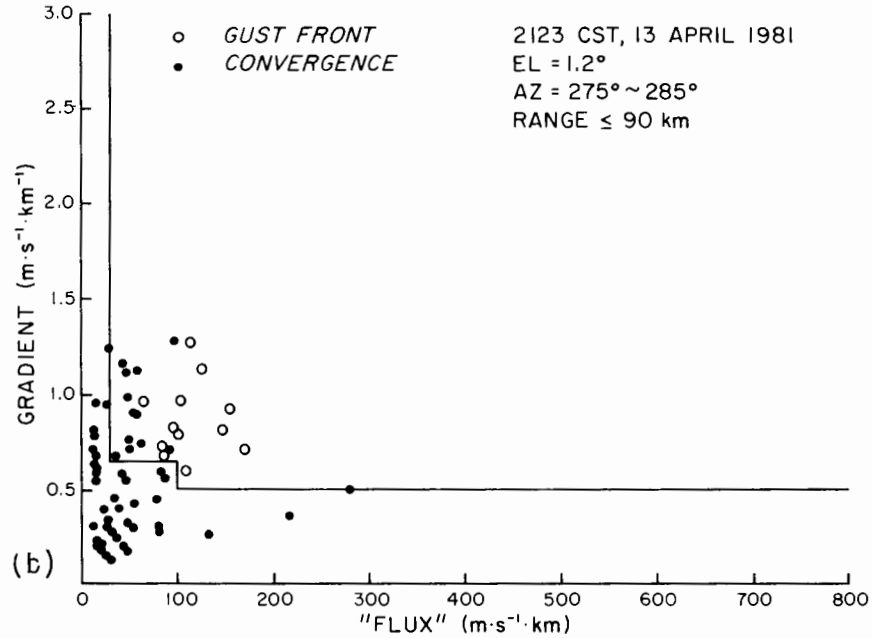

Figure 9 Detection region for pattern vectors in the gradient - "flux" plane. Data are for the April 13, 1981, portion of the front extending over 10° in azimuth that was (a) perpendicular to the radials and (b) almost parallel to the radials.

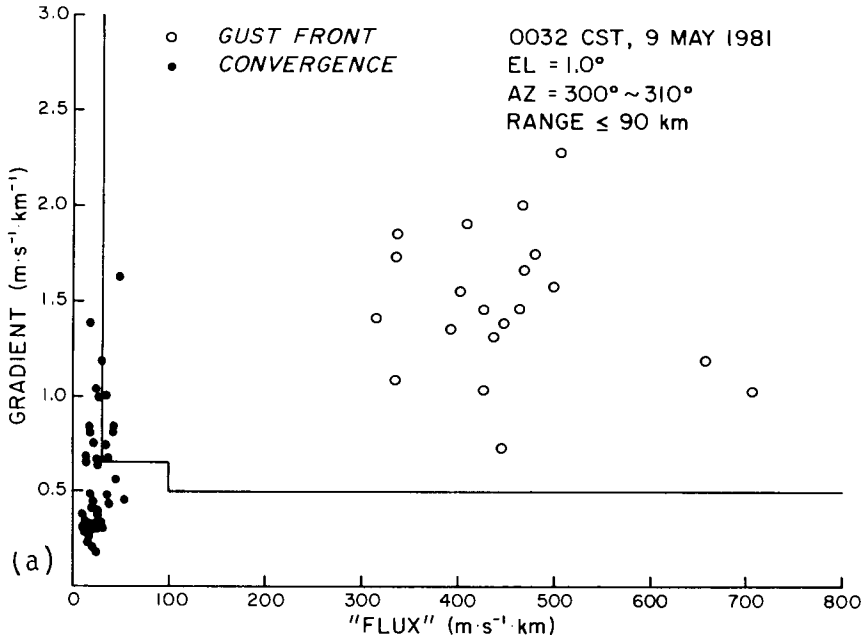

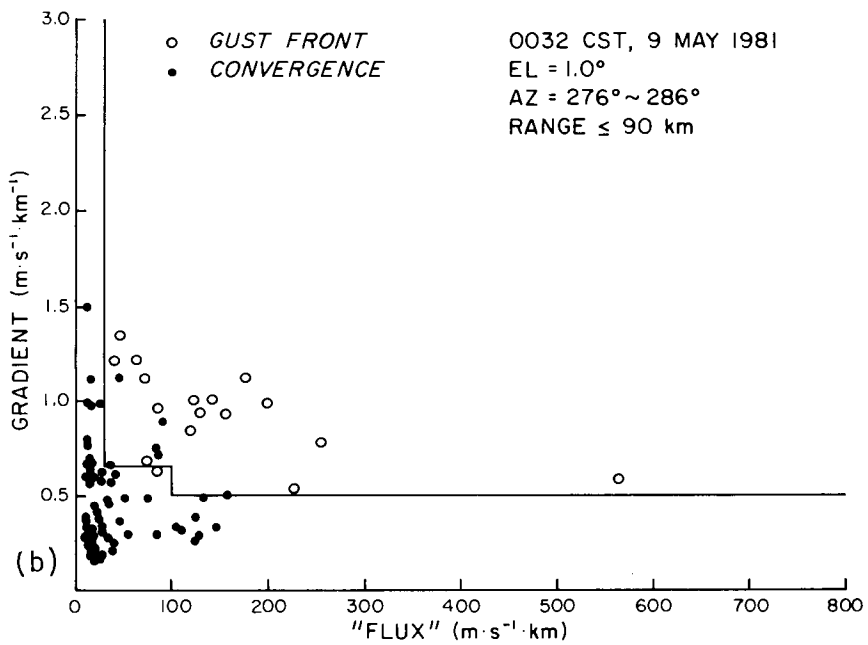

Figure 10 Detection region for pattern vectors in the gradient - "flux" plane. Data are for the May 9, 1981, portion of the front extending over 10° in azimuth that was (a) perpendicular to the radials and (b) almost parallel to the radials.

April 13, 1981, and May 9, 1981. They did work well for two other cases that we analyzed.

3.5 Detection of Azimuthal Shear

It is possible to detect fronts that are tangent to radials if the mesocyclone algorithm (Zrnic **et al.**, 1984) is used. This is because the converging winds on either side of the line are not perpendicular to the line; the environmental flow usually has a component along the gust; behind the gust the flow has a cyclonic curvature so that a cyclonic shear is seen in the mean velocity display. Anticyclonic shear may also characterize the transition between the environment and the outflow, especially if the wind shear vector progresses counterclockwise with height; at times there may be two almost parallel shear lines--one cyclonic, the other anticyclonic as produced by a downburst (Fig. 11).

We decided to adapt the mesocyclone shear algorithm so that it can detect azimuthal shear near the ground. Because cyclonic shear is prevalent and because of time constraints, we made modifications to detect only cyclonic shear. The main changes needed for low-level shear are the thresholds listed in Table 2. These were obtained after several trials with a limited number of data. Note that the reflectivity threshold is -15 dBZ and that shear and momentum thresholds are about half those for detecting mesocyclones and shears aloft. An example of the detection region in the shear momentum plane (Fig. 12) shows the expected distinction between pattern vectors of gust shear lines and other shears. Even though there is some overlap, the additional criteria such as proximity (for sorting) and shape of sorted features eliminate most of the false or insignificant shears. In order to reduce memory storage and speed up the computations, we examined azimuthal shears at every fourth range location (gate). This, together with the minimum number 10 (Table 2) of pattern vectors in a feature, means that only shear lines at least 4 km long are considered. Maximum radial distance for classifying adjacent vectors in the same feature is also 4 km, and the azimuthal separation is 3.3°. This last value was obtained by considering the separation between radials, which for our data is 1°. So the vector centers may be misaligned by at most three radials. As in the gust front algorithm based on convergence detection, a feature should not contain more than one pattern vector at a fixed range. Thus, if more than one such vector is sorted into a feature, it must be separated and put into a new feature.

TABLE 2

Thresholds for Detecting Azimuthal Shear Lines

	THRESHOLD	NUMERICAL VALUES
L_s	Low shear	$1.5\ m \cdot s^{-1} \cdot km^{-1}$
H_s	High shear	$2.0\ m \cdot s^{-1} \cdot km^{-1}$
L_m	Low momentum	$25\ m \cdot s^{-1} \cdot km$
H_m	High momentum	$50\ m \cdot s^{-1} \cdot km$
D_r/D_a	Ratio of feature length, D_r, to feature width, D_a	$\geqslant 3$
M	Minimum number of vectors allowed in a feature	10
l_a	Maximum distance between the azimuthal centers of two vectors for classification in the same feature	3.3°
l_r	Maximum radial distance between two vectors	4 km
Z_t	Reflectivity threshold	-15 dBZ
h	Height threshold	$\leqslant 3$ km

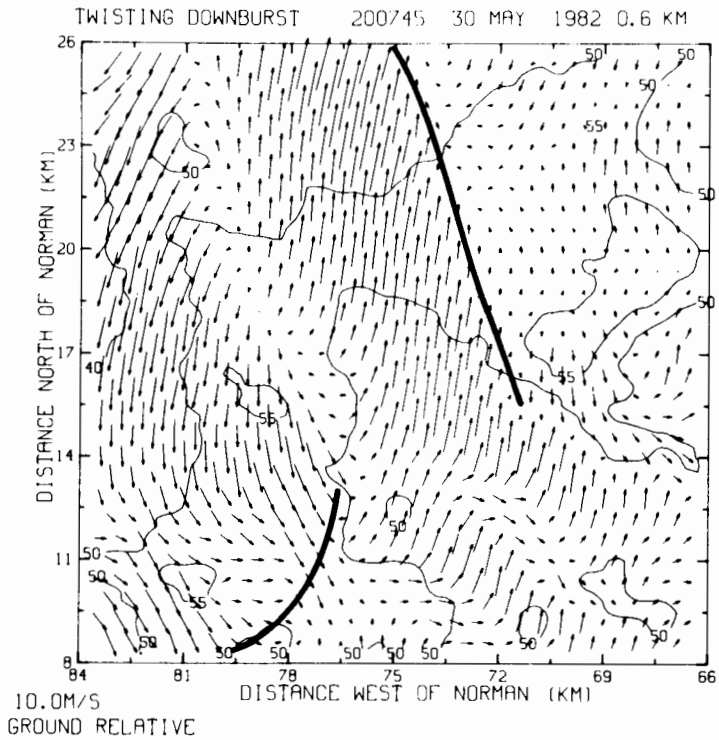

Figure 11 Twisting downburst of May 30, 1982. The center of this downburst is at -80 km, 18 km from the Norman radar. Wind vectors were obtained from data of two Doppler radars, and the scale vector is indicated in the lower left corner. This downburst is imbedded in strong reflectivities as seen from the extent of the 50 dBZ contour. The leading edge of the outflow NE of the center (thick line) would exhibit anticyclonic shear to any radar located north or south of it. Parallel to this line and about 3 km west of it the radars would detect a cyclonic shear. (Courtesy Mike Eilts, NSSL).

3.6 Tracking of Gust Fronts

Once the gust front feature has been identified, there are several options for displaying and tracking it. In order to display the front at sites remote from the main computer, it is desirable to characterize the front's shape with a small number of parameters. We have found that with a convergence algorithm a least-squares fitted curve,

$$r = A\theta^2 + B\theta + C \ , \tag{17}$$

can be used very effectively both to display the front and to extrapolate its position into the future. In (17) θ's are azimuths of pattern vectors and r's can be either the average value, $(r_b + r_e)/2$, of the pattern vector range or the range to the maximum gradient of a pattern vector. It is shown in later sections of this report that the locations of maximum gradients characterize better the frontal discontinuity. To test the goodness of fit, the root mean square (RMS) or standard error between the fitted curve and data is computed. In order to track the front, its range center (6) and azimuth center (5) at two consecutive times t_1, t_2 are needed. Then, assuming that the front's propagation velocity equals the velocity at which the center is

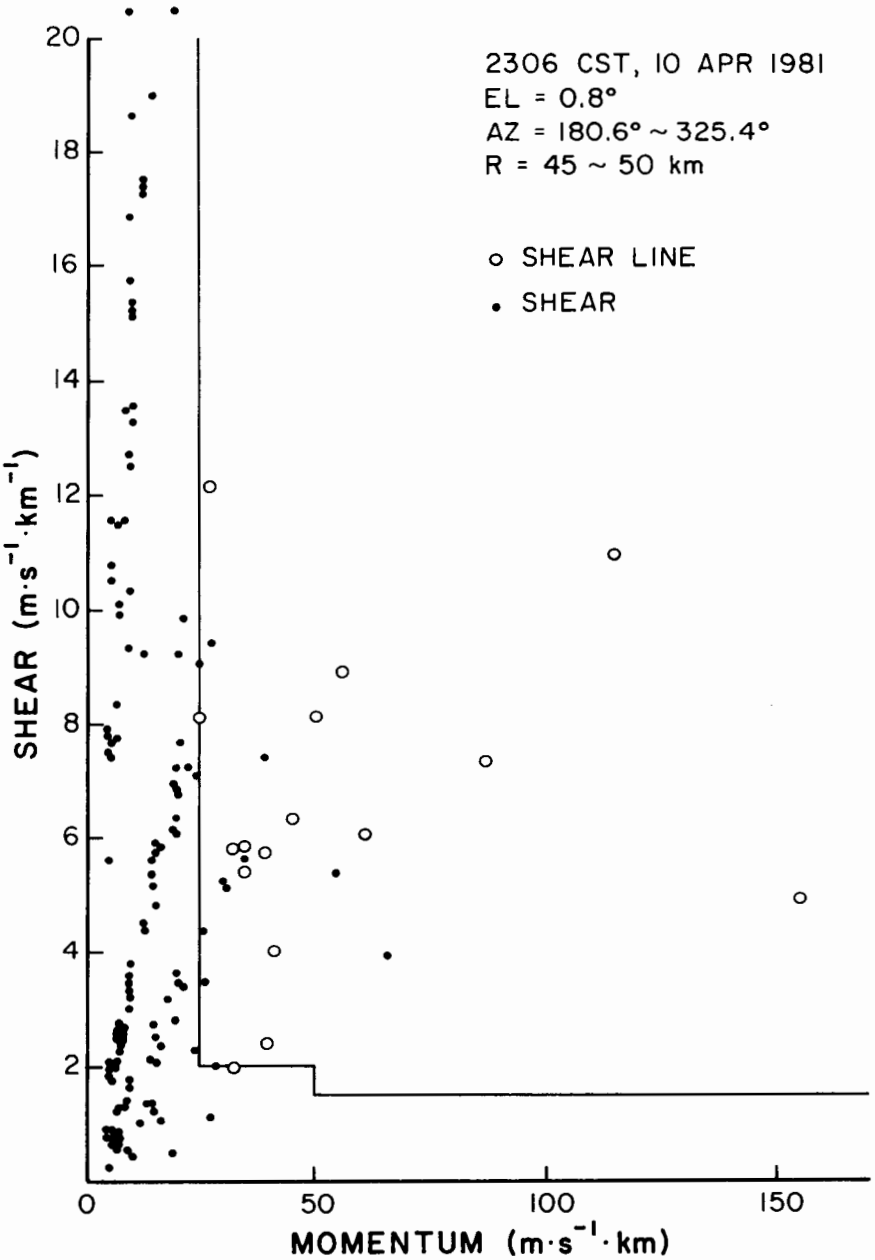

Figure 12 Detection region for the pattern vectors in the shear momentum plane applicable to the mesocyclone shear algorithm. Data are for the indicated portion (azimuth, range) of the front of April 10, 1981.

moving, the front's position can be projected for later times. This is done by advecting the curve (17) at a time t_2 with the estimated propagation velocity. For azimuthal shear lines detected by the mesocyclone-shear algorithm, it is natural to regress θ on r because θ has a quadratic dependence (arc) on r. So we use

$$\theta = Ar^2 + Br + C \tag{18}$$

where the data pairs (θ_i, r_i) are the centers of pattern vectors.

4. Case Studies

In this section we examine the performance of our algorithm on five different cases. As ground truth we use the positions of the gust as indicated by the velocity discontinuities on color displays and on contour plots. We also show examples of tracking and outputs such as feature area, "flux", and gradient as a function of range.

4.1 April 13, 1981

A very intense front developed in a squall line that passed by some surface stations and over the Cimarron radar site on this day (see Fig. 10 in Zrnic' and Lee, 1983). We applied the algorithm to seven scans (Table 3) and chose three consecutive scans at 1.2° in elevation to illustrate detection and tracking. The mean velocities for the last scan (2123 CST) are shown in Fig. 13. Note the arc shape of the frontal discontinuity in the velocity field and the richness of velocity structure suggestive of turbulent eddies, which are also present in the spectrum width display (see Zrnic' and Lee, 1983). We superposed the gust front position on the velocity contours to obtain Fig. 14. There the deduced front's shape follows quite well the $-10\ m \cdot s^{-1}$ velocity contour and is at the locations that one would subjectively determine from the color display. Note that the arc stops at 40 km to the west of radar and about 30 km to the north. From the color display we infer that the front extends beyond these ranges, but because it becomes tangential to the radial, it cannot be detected with radial convergence measurements.

In Fig. 15 we show the fronts detected at an elevation of 0.8°. Locations of maximum gradients and their five-point running averages are plotted. Also superposed are the least-squares fitted positions. There are four frontal lines, but only two (labeled 1 and 2) had time and height continuity. The longer line closer to the radar (1 in Fig. 15) is the primary gust, and the one behind (number 2) is a secondary surge. We made these deductions by examining time and height continuity (Figs. 16a and b). At 1.3° in elevation (Fig. 16a) there are three gusts that have temporal continuity (labeled 1, 2, 3) over three scans. These gusts exhibit also height continuity as seen in Fig. 16b, where the secondary surges (2 and 3) are found at four elevation angles and the primary surge is present at all five elevations examined. The other unmarked shears are transient and must be eliminated from displays. It suffices to check the continuity of range and

TABLE 3

Parameters for the April 13, 1981, Front

TIME (CST)	ELEVATION ANGLE (deg)	RANGE OF CENTER (km)	HEIGHT OF CENTER (km)	AVERAGE OF MAX GRADIENT ($m \cdot s^{-1} \cdot km^{-1}$)	AVERAGE OF "FLUX" ($m \cdot s^{-1} \cdot km$)	LENGTH (km)	RMS ERROR (km)
2111	1.3	39	0.97	6.4	234	30	0.8
2116	1.3	33	0.82	6.5	217	39	1.0
2123*	0.4	25	0.21	5.9	221	21	1.2
		26	0.22	6.2	365	21	1.5
2123	0.8	25	0.38	5.4	352	38	1.4
2123	1.2	26	0.58	5.3	305	44	1.5
2124	2.0	24	0.88	6.0	262	32	1.1
2124	2.8	25	1.23	5.6	83	12	1.5
AVERAGE		28		5.9	255	30	1.3

*In this scan the algorithm separated the gust into two lines.

azimuth centers (Eqs. 5, 6) of gust lines. The continuity should extend through two to three lowest elevations. In order to establish track the front must be detected at least in two consecutive scans at the same elevation.

Three consecutive positions of the front are shown in Figs. 17a and b. Both the fitted curve and the centers of pattern vectors that were used as data for the fitted curve are drawn in Fig. 17a. In Fig. 17b we used the locations of maximum gradients to trace the front and perform the fitting. From the visual comparison of the two figures it is obvious that the maximum gradients produce a smoother trace, which is also confirmed from the standard error between data and the fitted curves (Fig. 18a, b). These errors are at least two times lower when maximum gradients are used and do not exceed 1.5 km (Table 3). With the dashed line we have indicated errors when the pattern vectors belonging to a secondary surge were not separated from the feature and

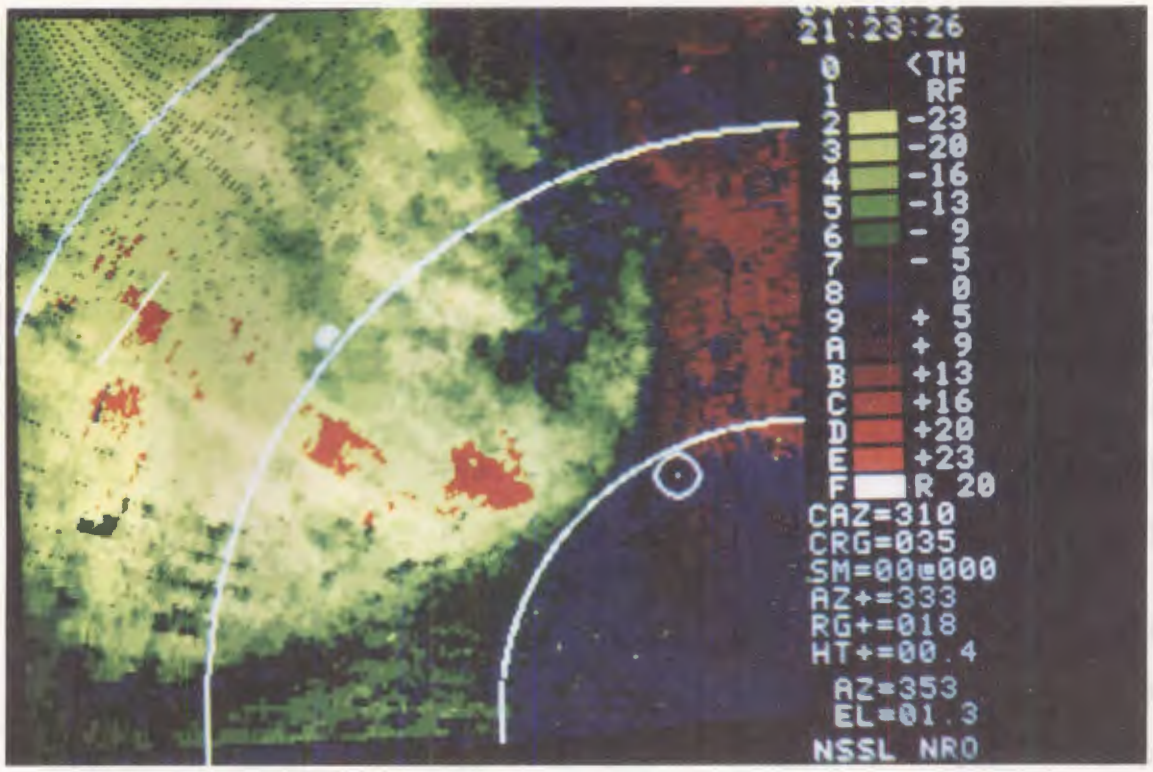

Figure 13 Doppler velocities for the gust front of April 13, 1981. Elevation is 1.3°, range marks are 20 km apart, and red represents velocities away from the radar. Patches of red in the middle of green are aliased velocities, most likely due to outflow produced by intense downdrafts.

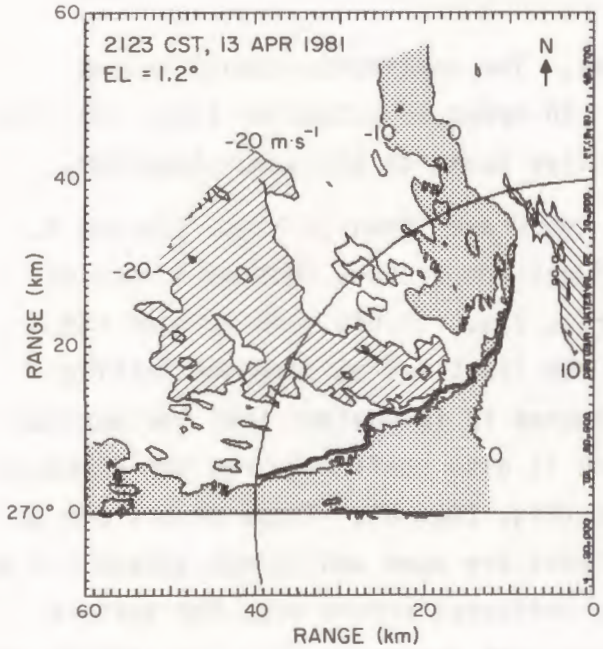

Figure 14 Contours of mean Doppler velocities for the gust front of April 13, 1981. The contour interval is 10 $m \cdot s^{-1}$. Objectively determined location of the front (thick line) is superposed. The square next to C is at the center (r_c, az_c) of the front.

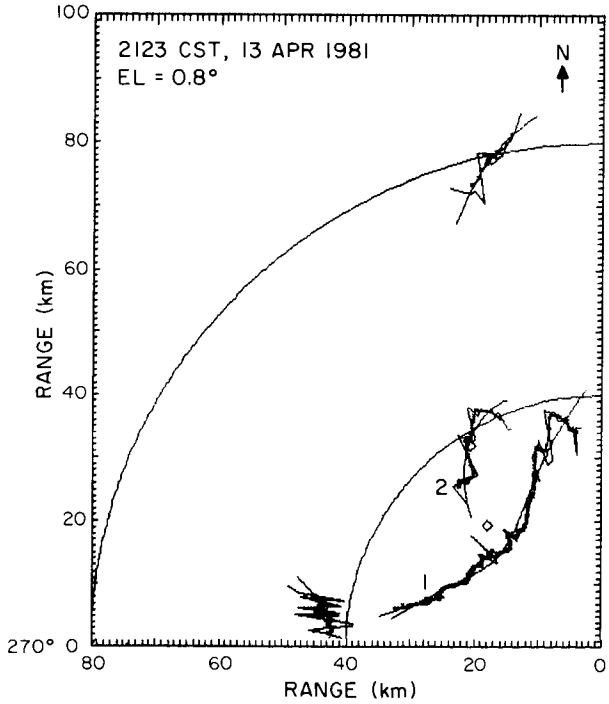

Figure 15 Detected gusts at an elevation of 0.8° for the front of April 13, 1981. The locations of maximum gradients and their five-point running averages are plotted. Superposed also are the least squares fitted lines. The primary gust is labeled with 1 and the secondary surge with 2.

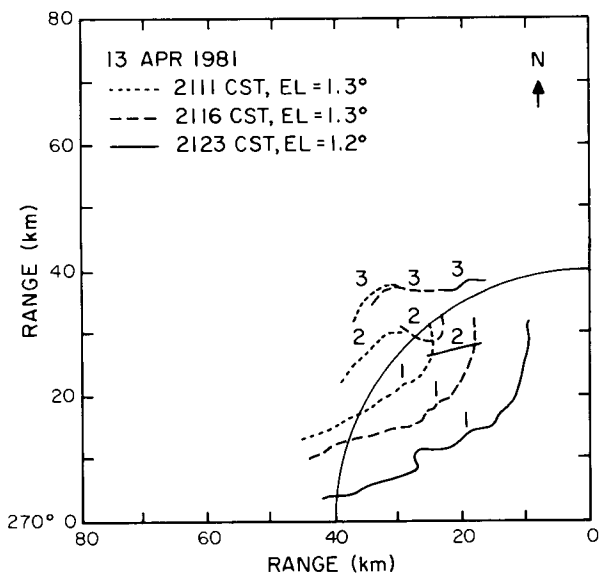

Figure 16(a) Detected gust lines at a constant elevation of 1.3° at three consecutive times. The lines are five-point running averages of maximum gradient locations. Numbers 1, 2, and 3 identify features with time continuity.

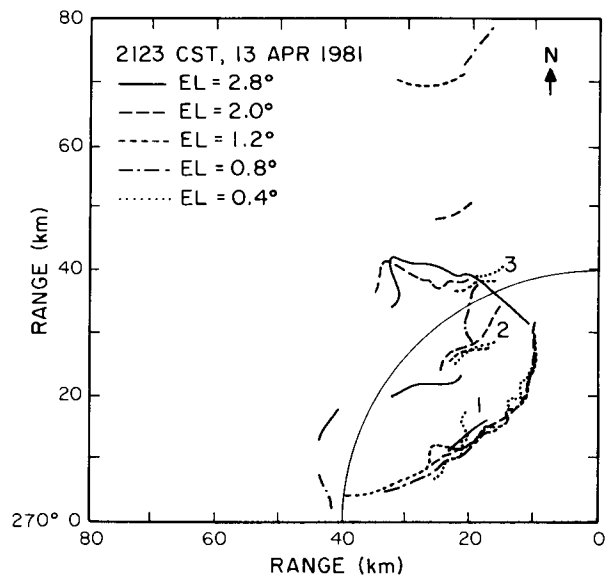

Figure 16(b) Detected gust lines in one volume scan. Numbers 1, 2, and 3 correspond to the same features as in Fig. 16a, which are continuous through four heights.

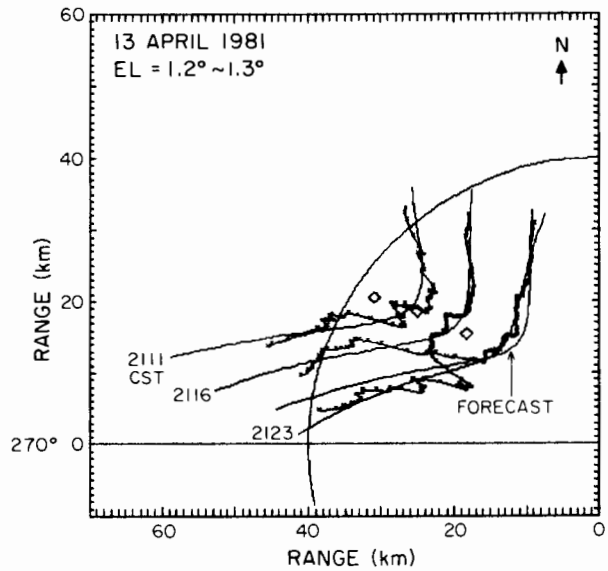

Figure 17(a) Three consecutive positions of the front (April 13, 1981). The smooth curves are least squares fits to the data, and the forecast position is indicated. The range mark is at 40 km from the radar. Centers of the pattern vectors were used to trace the gust. Squares indicate the centers of these three front lines.

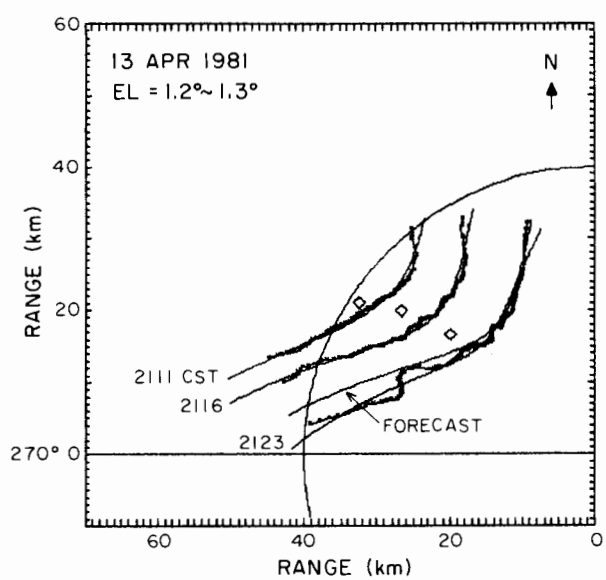

Figure 17(b) Consecutive positions of the front, as in Fig. 17a except that locations of maximum gradients were used to trace the gust.

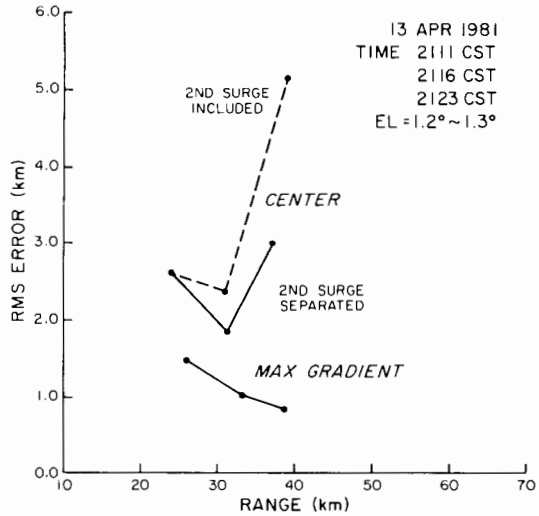

Figure 18(a) RMS error between the fitted curve (primary gust) and (1) center of pattern vectors and (2) locations of maximum gradients. Data are from three consecutive times (ranges) for April 13, 1981. The range is to the centers of features, which differ slightly for the two methods.

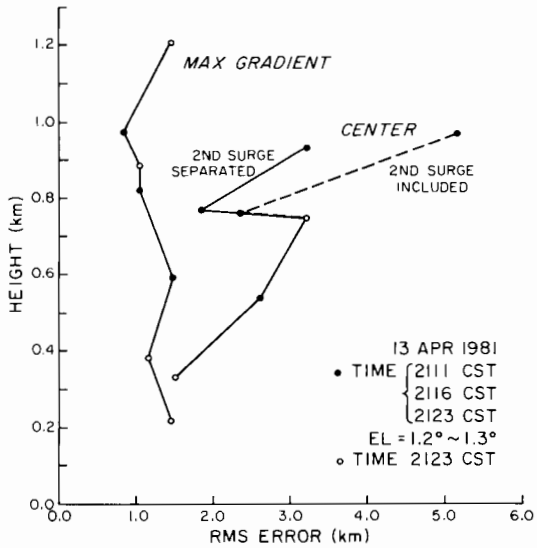

Figure 18(b) Full circles are RMS errors as in Fig.18a, plotted versus height. Open circles are RMS errors for the gust front at other than 1.2-1.3° in elevation; these are not plotted on Fig. 18a.

the center of vectors was used to locate the front. Similar increase in errors (not shown) occurs when the secondary surge is not separated in the maximum gradient method. It is not surprising that the maximum gradients are better locators of the frontal discontinuity than centers of the pattern vectors. Physically it is the maximum gradients that define fronts whereas the centers of pattern vectors only approximate frontal discontinuities. Our main reason for trying centers of pattern vectors was ease of calculations. Finding maximum gradients requires an additional pass through the velocity data contained between r_b and r_c of a pattern vector. Because in this and other tested cases detection and tracking based on maximum gradients of pattern vectors outperformed the method based on centers of the pattern vectors, we consider only the former in the remainder of this report.

The forecast position of the front (Fig. 17b) is in reasonable agreement with the actual position; maximum displacements between the two are less than 4 km. To improve further the forecast positions would require intervals shorter than 5-7 min between scans. The values of average gradient, average "flux", average of maximum gradients, and area depend on the development stage of the front (Fig. 19a). The area may tend to increase closer to the radar if elevation is constant because more pattern vectors that would otherwise fall below the beam can be detected. Average gradients between 1.5 and 2 $m \cdot s^{-1} \cdot km^{-1}$, maximum gradient larger than 5 $m \cdot s^{-1} \cdot km^{-1}$, and fluxes between 100 and 400 $m \cdot s^{-1} \cdot km$ are typically encountered in strong gusts; this is illustrated in Table 3 and in Fig. 19b where these attributes are plotted versus height. The lengths in Table 3 were measured along the least squares fitted line, and we note that they exceed 20 km at the lower elevations. This observation may be useful for discriminating significant fronts.

Because the frontal discontinuity on this day extended also along a radial (Fig. 13), we ran the modified mesocyclone shear algorithm to see how it would detect and connect the azimuthal shear to the radial convergence. Results for the three scans are extremely promising (Fig. 20a). Gust positions estimated from convergence and from azimuthal shear join smoothly and even overlap a bit. In this example the forecast position (Fig. 20b) differs considerably (2 to 10 km) from the actual position of the front; however, the forecast from the convergence algorithm is very good (Fig. 17b) so that the overall error with the two algorithms working together is much less.

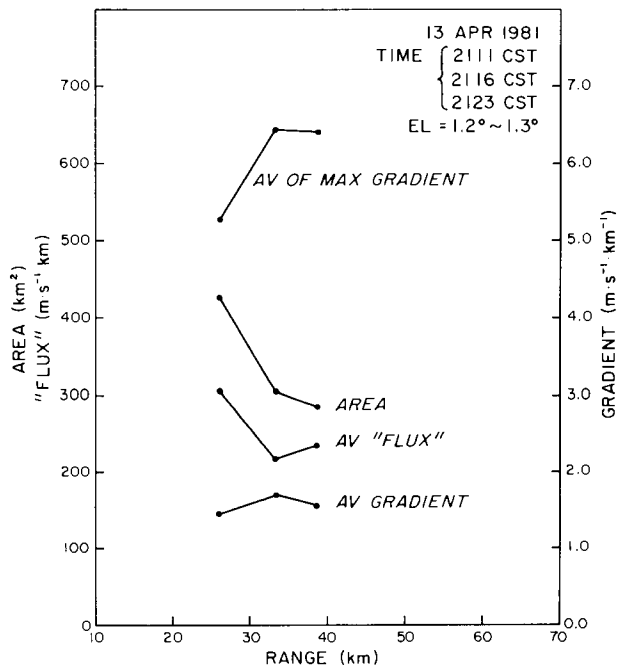

Figure 19(a) Area, average "flux", average gradient, and average of maximum gradients versus range for the gust of April 13, 1981.

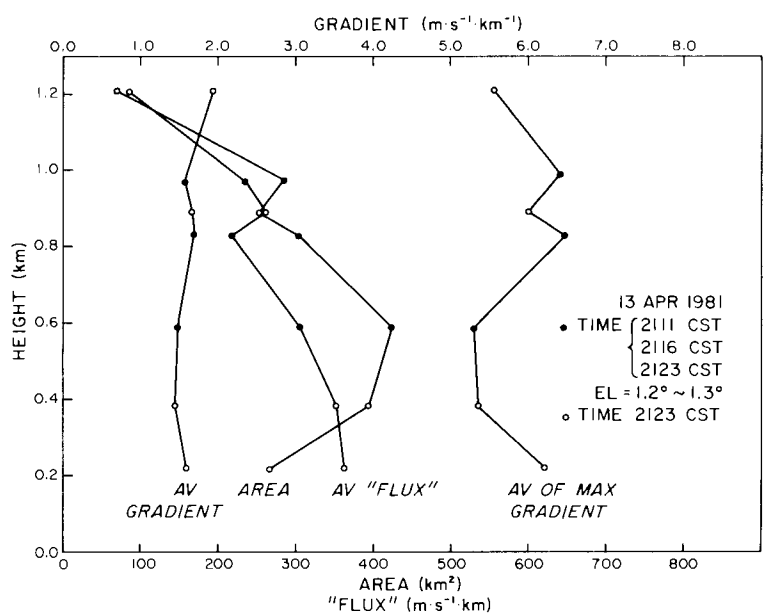

Figure 19(b) Parameters as in Fig.19a, plotted versus height.

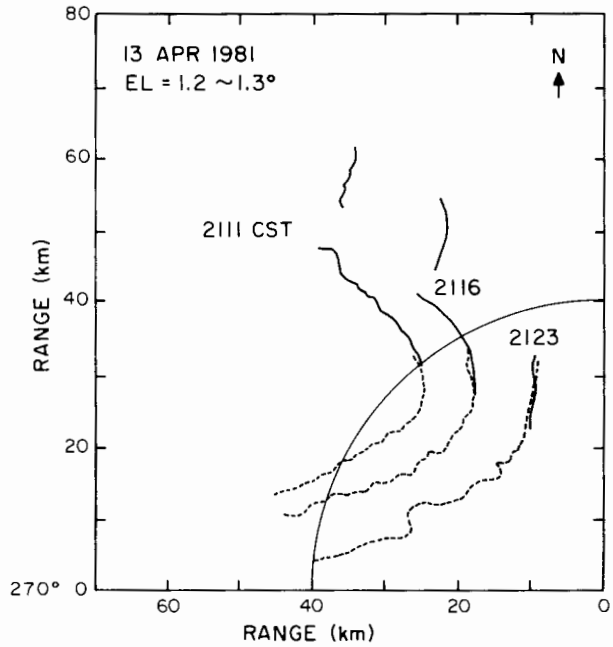

Figure 20(a) Detected gust fronts. Dashed line is a five-point running average of maximum gradient locations (from convergence algorithm, same as "1" on Fig. 16a) and the solid line is a five-point running average of pattern vector centers (from mesocyclone-shear algorithm).

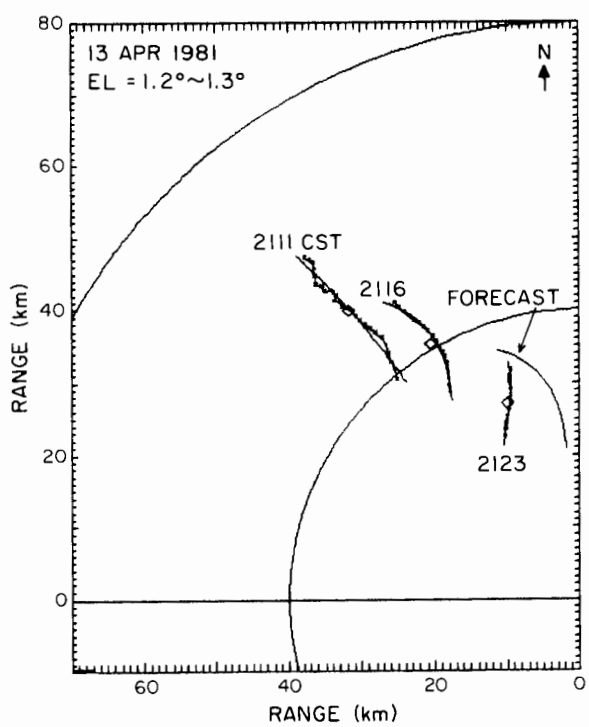

Figure 20(b) Actual positions of the gust and a forecast position obtained from the mesocyclone-shear algorithm.

4.2 May 9, 1981

This front had a well-defined thin line at the leading edge, thought to be generated by debris made airborne by the strong gust winds immediately behind the front (see Fig. 12a in the report by Zrnic' and Lee, 1983). In this case the strong shear regions were 10 km ahead of the higher reflectivity regions associated with precipitation. The frontal boundary in the mean velocity display (Fig. 21) is quite distinct, but it becomes diffused in the spectrum width display because the width is more susceptible to contamination from the ground clutter (Fig. 12d in Zrnic' and Lee, 1983).

A large portion of the front is detected by the algorithm (Fig. 22), and its shape follows faithfully the -10 $m \cdot s^{-1}$ velocity contour. Again, portions of the front that are aligned along radials are not detectable. Several gust lines detected at an earlier time are shown in Fig. 23. Only those numbered 1 meet the time and height continuity criteria. They are part of the same front, but the algorithm fails to connect them because they are separated by a region of weak gradients of radial velocities. The feature beyond 80 km could be a shallow gust that dissipated before subsequent scans were made.

The results of least squares fitting this front (Fig. 24 and Table 4) and tracking it are very similar to the April 13 case. Noteworthy is a very tight fit at farthest range. The forecast position deviates from the true position by at most 2 km even though the time interval between scans are twelve and fourteen minutes. Standard errors (Fig. 25) and area, average flux, average gradient, and average of maximum gradients (Fig. 26) show very similar behavior as for the April 13 gust, not only in general trends but also in values. This reinforces our belief that the algorithm is consistent and will reproduce similar results on other bow-shaped gusts.

4.3 May 29, 1980

We chose this gust (Fig. 27) for two reasons: (1) It was moving away from the radar, and we wanted to see how the algorithm would perform in such a situation. (2) It had a "line echo wave pattern" with a cyclonic couplet. This front is also discussed by Zrnic' and Lee (1983), who show the three moments on their Fig.7. The gust front algorithm has no provision for circulation detection, but in an operational setup several algorithms that detect and track hazardous weather features must be used concurrently. Thus, a composite of hazards needs to be presented to operators for further

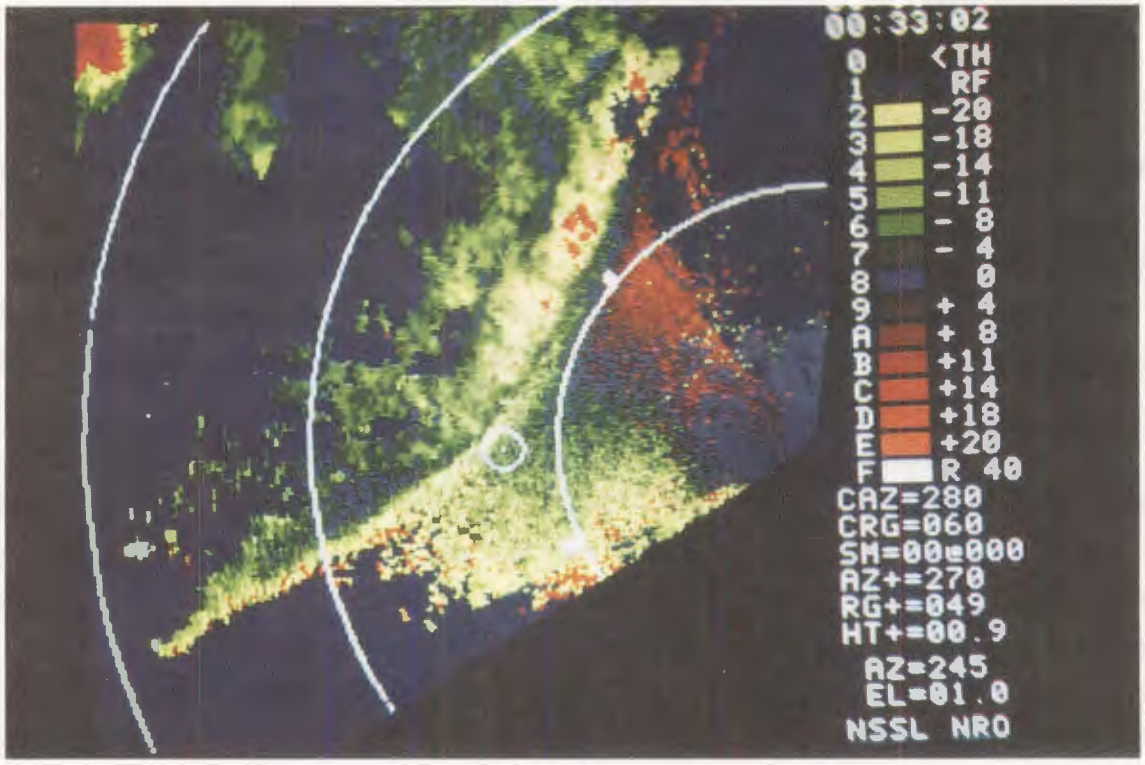

Figure 21 Doppler velocities for the gust front of May 9, 1981. Range marks are 40 km apart, elevation is 1°, and the cursor is near the center of the front.

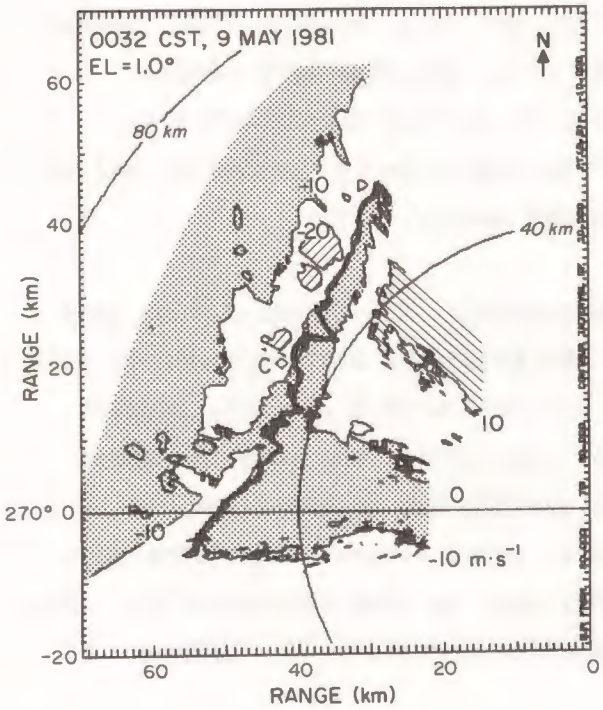

Figure 22 Contours of mean Doppler velocities for the gust front of May 9, 1981. The contour interval is 10 m·s^{-1}. Objectively determined location of the front (thick line) is superposed.

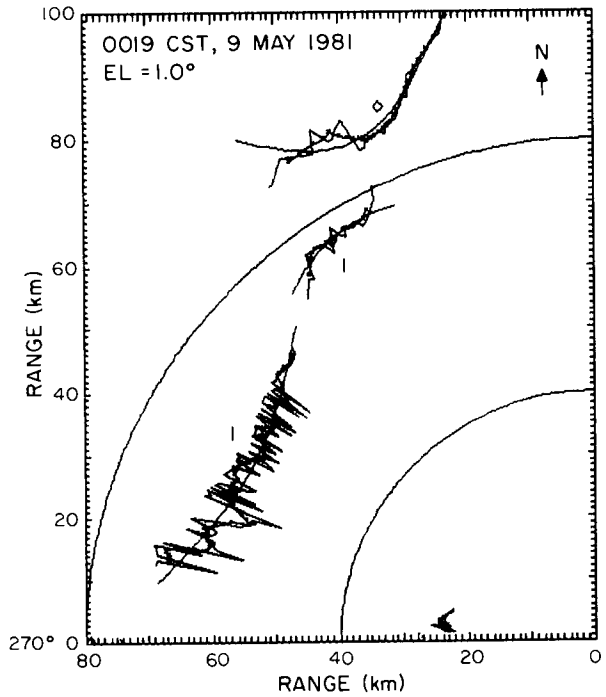

Figure 23 Detected gust lines at a constant elevation of 1°. The curves labeled "1" are part of the same gust. Locations of maximum gradients, their five-point averages, and least squares fitted positions are plotted.

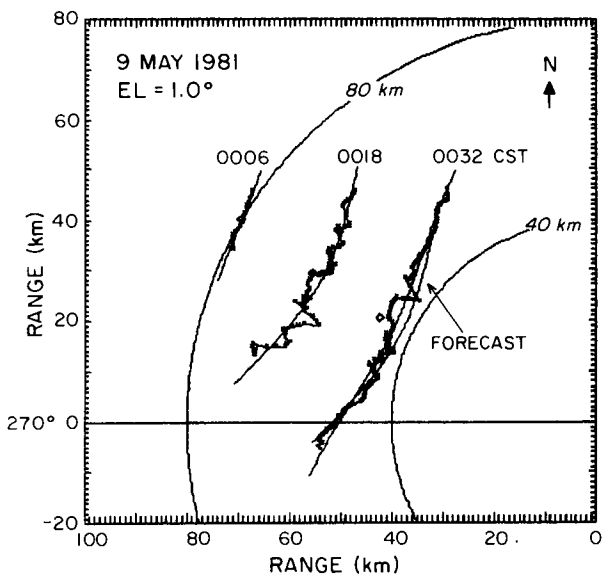

Figure 24 Three consecutive positions of the front on May 9, 1981. The smooth curves are least square fits to data, and the forecast position is indicated.

TABLE 4

Parameters for the May 9, 1981, Front

TIME (CST)	Elevation ANGLE (deg)	RANGE of CENTER (km)	HEIGHT of CENTER (km)	AVERAGE OF Max GRADIENT ($m \cdot s^{-1} \cdot km^{-1}$)	AVERAGE of "FLUX" ($m \cdot s^{-1} \cdot km$)	LENGTH (km)	RMS ERROR (km)
0006	0.5	83	1.13	5.5	138	64	1.7
0006	1.0	80	1.77	6.4	79	13	0.8
0018	0.5	65	0.81	4.9	411	62	2.7
0019	1.0	63	1.33	4.6	205	45	3.3
0032	1.0	47	0.95	4.6	321	58	1.8
AVERAGE		68		5.2	231	48	2.1

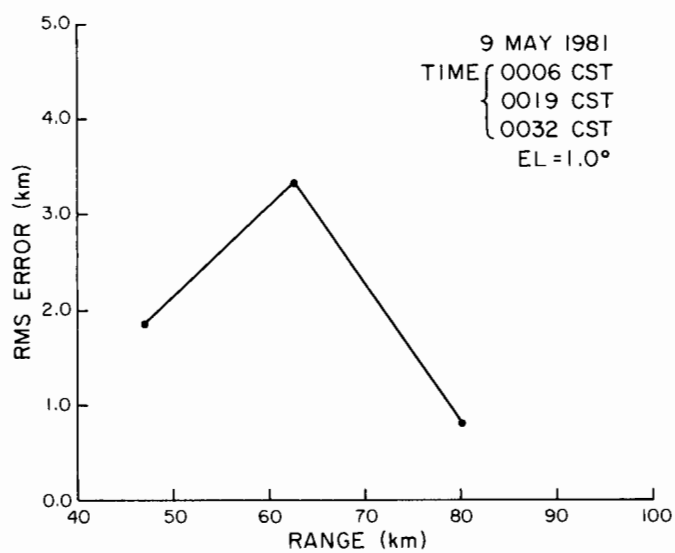

Figure 25 RMS error between the fitted curve and gust positions determined by the location of maximum gradients for May 9, 1981.

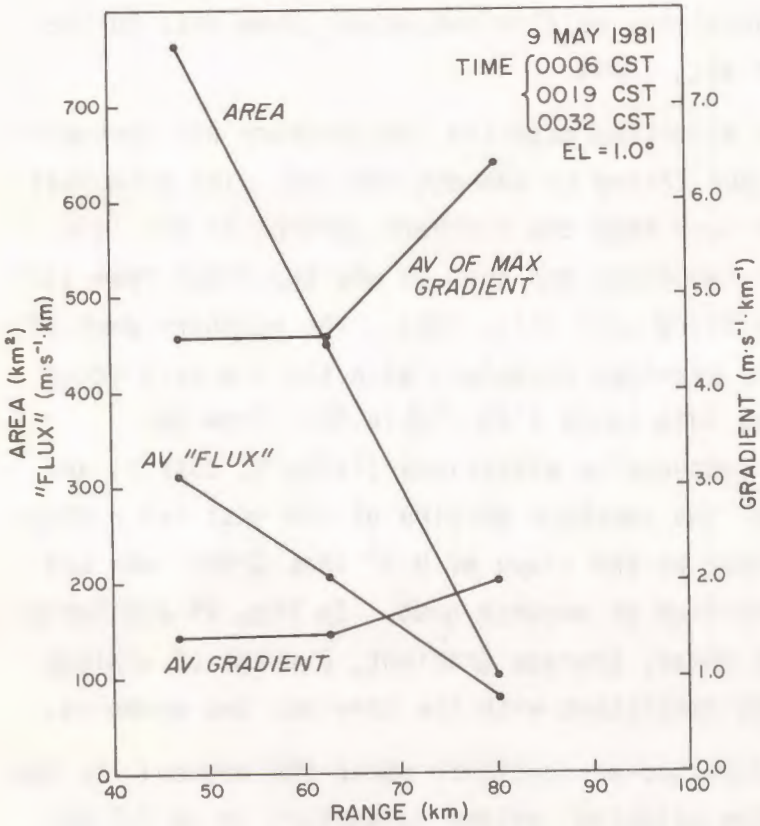

Figure 26 Area, average "flux", average gradient, and average of maximum gradient versus range for the gust of May 9, 1981.

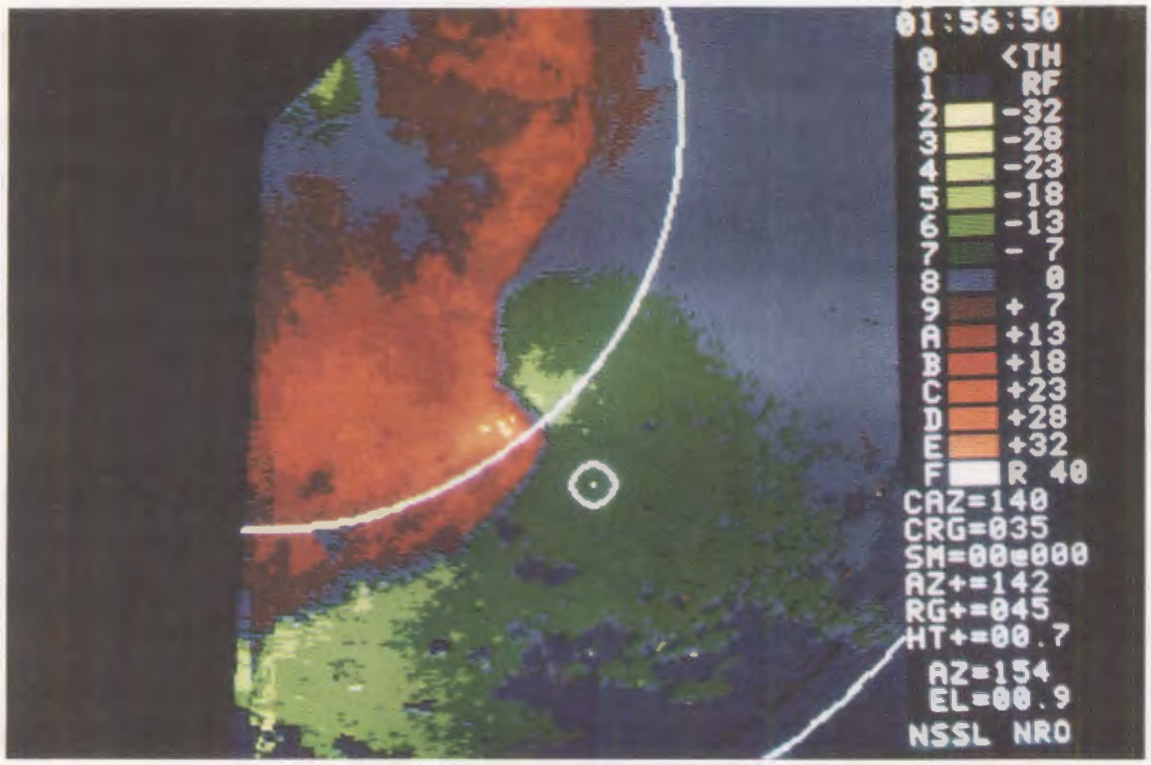

Figure 27 Doppler velocity display for the gust front of May 29, 1980. Range marks are 40 km apart, elevation is 0.9°, and the cursor is near a low-level vortex.

interpretation and warnings. Therefore, we also subjected these data to the mesocyclone algorithm (Zrnic' **et al.,** 1984).

As expected, the gust front algorithm detected the southern and northern portions of the wave (Fig. 28a) but failed to connect the two. The azimuthal limits of the radar antenna were such that the southern portion of the line was not covered during the first two scans and that is why the front from 140° to 180° was detected only in the third scan (Fig. 28b). The northern part of the line tracks as well as in the previous examples, with the standard error between the fitted curves and the data below 1 km (Table 5). From the position of the center at three consecutive elevations (Table 5, case b) and plots (not shown), we deduce that the southern portion of the gust had a slope of about 7.5°, which is quite close to the slope of 8.5° that Zrnic' and Lee (1982, Fig. 6) show in a cross section of another gust. In Fig. 29 and Table 5 we show that the area, average shear, average gradient, average of maximum gradient, and RMS errors are also consistent with the previous two examples.

The mesocyclone algorithm detected mesocyclonic shear (M) between the two lines (Fig. 28). It estimated the azimuthal extent (diameter) to be 2.3 km and the radial 2.4 km, which enabled us to draw the core with the small circle. The outer circle has a diameter three times larger than the core because that is where the cyclonic circulation usually merges into the environmental flow (Lemon **et al.**, 1977). Because the circulation associated with fronts of this type is shallow (here less than 2.8 km) and because at low levels contamination with clutter may be substantial, height continuity should be used for confirmation of low level (less than 2 km) circulations only if the radar has a ground clutter canceller. But in either case, time continuity should be checked.

4.4 April 10, 1981

We chose the gust front from this day because the frontal discontinuity is parallel with radials (Fig. 30); hence, there is an ideal opportunity to test the new role of the mesocyclone-shear algorithm. Three volume scans were collected when the front was essentially parallel to the radial as in Fig. 30. The first two scans were about a minute apart and the third was six minutes after the second. The algorithm detected six shear lines at 2300 CST (Fig. 31a). Only the SE line (No. 1) is associated with a front. We emphasize that this line was broken into two segments when the radial distance, ℓ^r, between vectors for feature classification was 3 km and the

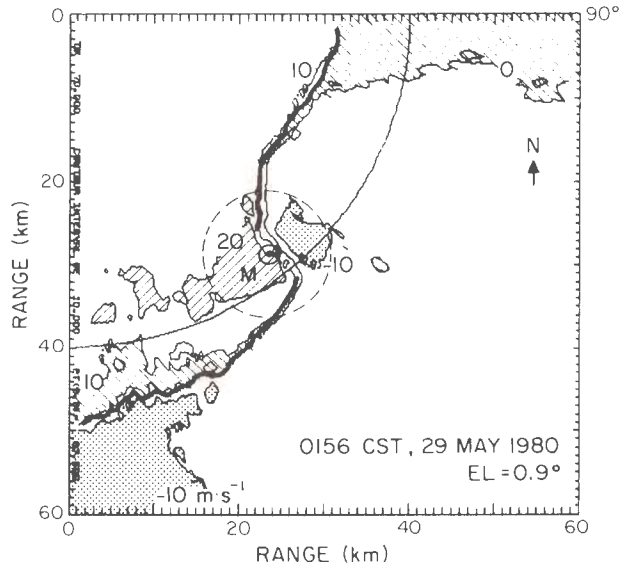

Figure 28(a) Contours of mean Doppler velocities of the gust front of May 29, 1980. The contour interval is 10 m·s^{-1}. Objectively determined location of the front (thick line) is superposed. The small circle indicates the core of a mesocyclonic vortex, and the dashed circle has a diameter three times larger than the core.

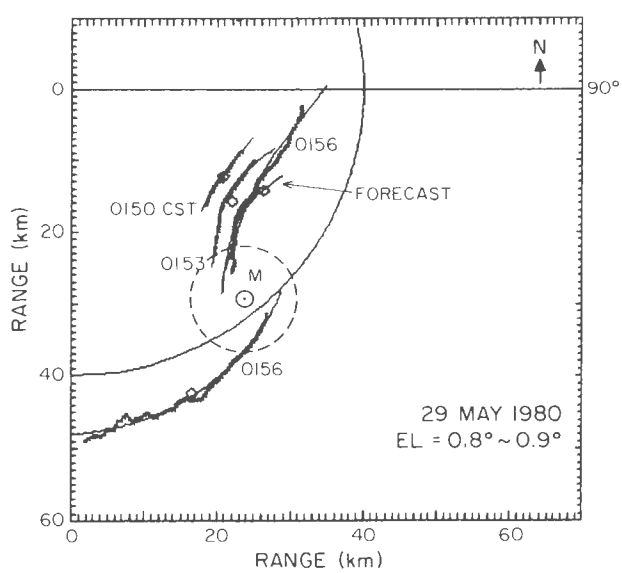

Figure 28(b) Three consecutive positions of the front on May 29, 1980. The smooth curves are least squares fits to the data, and the forecast position is indicated. The range mark is at 40 km from the radar.

TABLE 5

Parameters for the May 29, 1981, Front

TIME (CST)	ELEVATION ANGLE (deg)	RANGE OF CENTER (km)	HEIGHT OF CENTER (km)	AVERAGE OF MAX GRADIENT ($m \cdot s^{-1} \cdot km^{-1}$)	AVERAGE OF "FLUX" ($m \cdot s^{-1} \cdot km$)	LENGTH (km)	RMS ERROR (km)
0150	0.8	a. 24	0.37	8.5	303	12	0.2
0152	0.8	a. 26	0.40	9.3	373	20	0.4
0153	0.8	a. 27	0.42	9.5	355	19	0.2
0156*	0.5	a. 30	0.31	7.9	317	28	0.8
		b. 48	0.55	9.8	438	33	1.0
0156	0.9	a. 30	0.52	8.4	339	26	0.7
		b. 46	0.85	9.8	302	32	0.8
0157	1.3	a. 30	0.73	9.0	304	26	1.0
		b. 44	1.11	9.9	108	27	0.6
AVERAGE		34		9.1	335	25	0.6

*After this time the scan sector limits were increased and the algorithm detected both sides (a,b) of the line echo wave pattern.

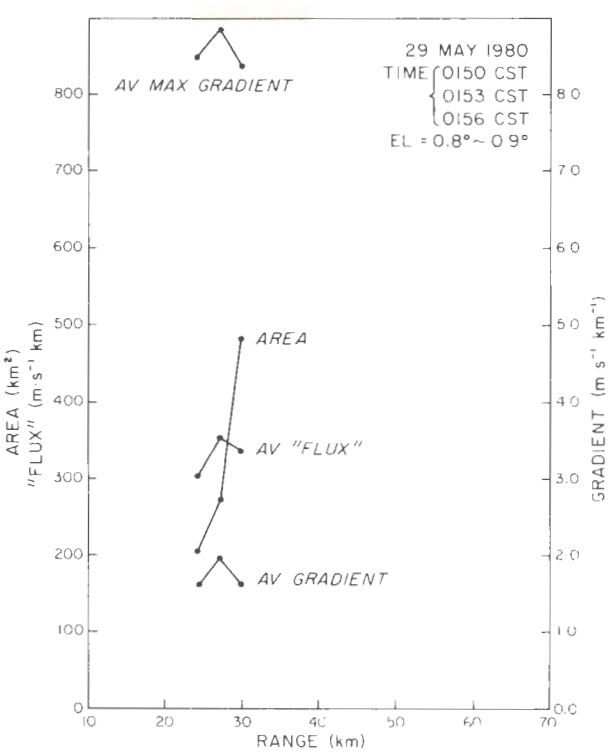

Figure 29 Area, average "flux", and average gradient versus range for the gust of May 29, 1980.

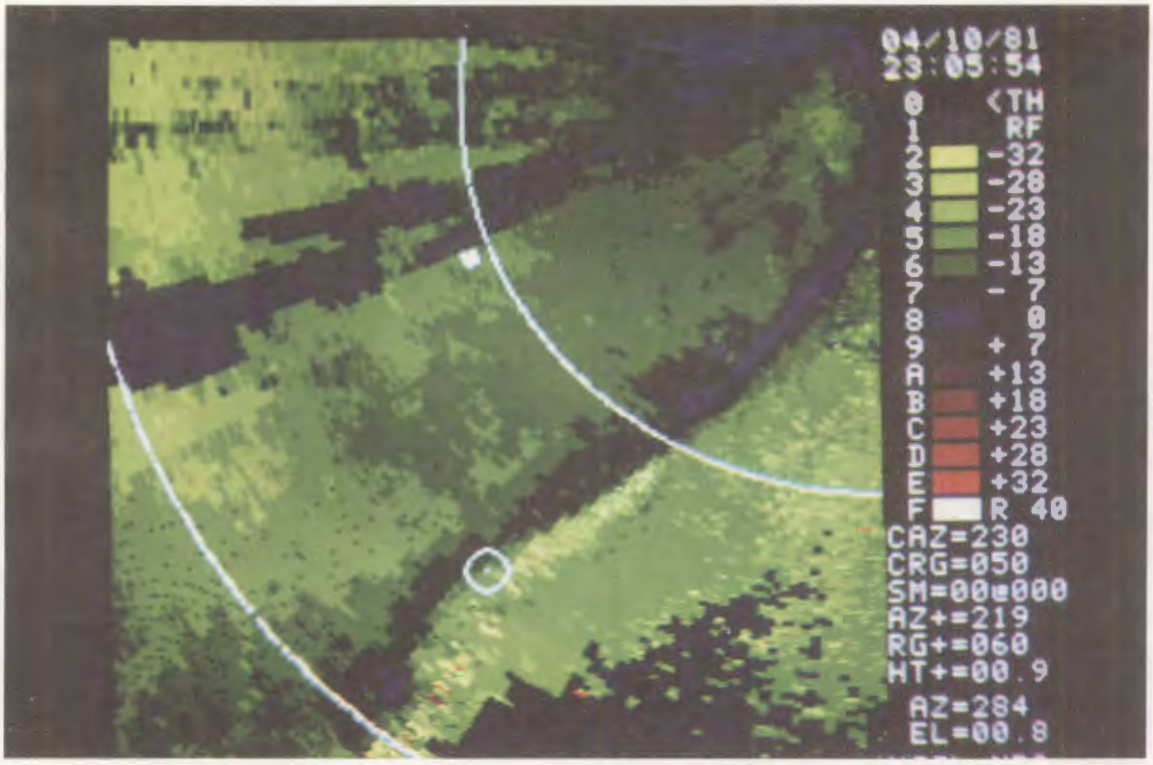

Figure 30 Display of mean velocities for the gust front of April 10, 1981. Range marks are 40 km apart, elevation is 0.8°, and the cursor locates the front. The area NW of the white square is contaminated with second-trip echoes.

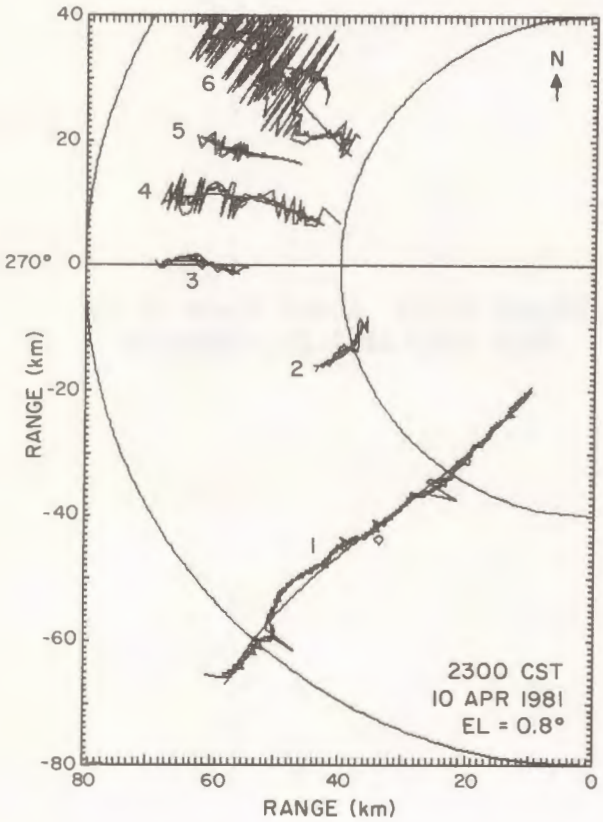

Figure 31(a) Shear lines detected by the mesocyclone-shear algorithm at 2300 CST on April 10, 1981, at 0.8° elevation. The data, their five-point average and the least squares fitted curves are drawn.

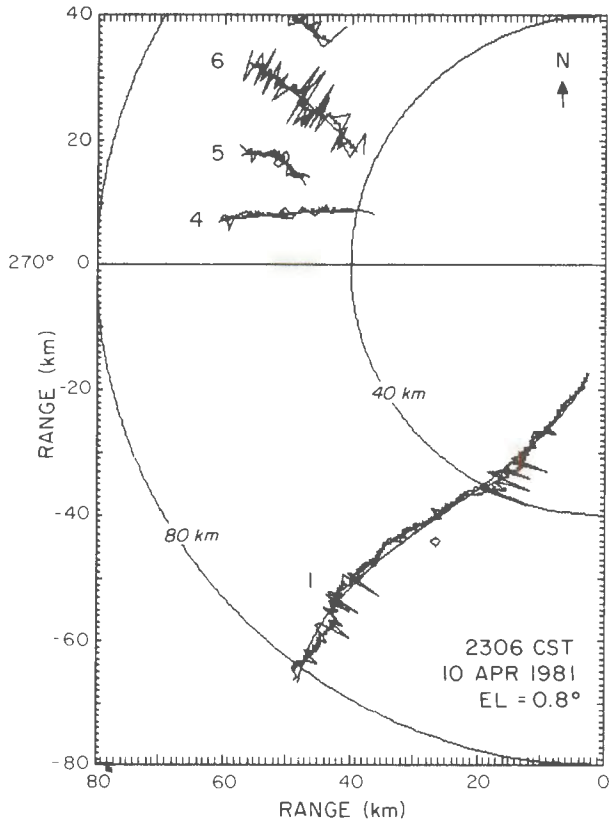

Figure 31(b) Shear lines as in Fig.31a, at 2306 CST.

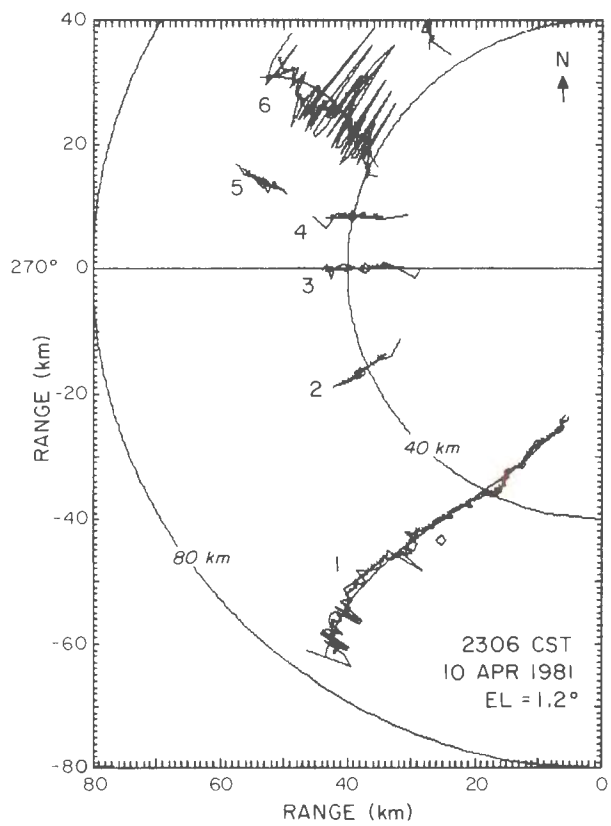

Figure 31(c) Shear lines as in Fig. 31b, at 1.2° elevation.

azimuthal separation was 2.2°. Also with these thresholds the total number of shear lines was eight. After changing the thresholds to 4 km and 3.3° (Table 2) the two segments connected and the total number of shear lines decreased. The long shear line farthest north (No. 6) is also genuine although it does not represent a strong gust but rather a weak transition between the environmental flow and the storm system. Its noisy appearance is due to the fact that pattern vectors from secondary surges at the same range are included in the feature. These could be separated in the same manner as that in the convergence algorithm. Other shear lines are spurious, caused mainly by the presence of second trip echoes that were overlaid in the NW quadrant. Only two of these spurious shears (No. 4 and 5 on Figs. 31a,b, and c) had time and height continuity (i.e., the centers were within 10 km). Thus, checks of time and height continuity must be made in order to reduce false alarms.

The shape and length of the detected front (No.1 in Fig. 31a and b) reproduced fairly well the discontinuity seen on the color display (Fig. 30). We were not able to track this front because the first two scans were very close in time, and the antenna was moving clockwise in one and counterclockwise in the other. So the front barely moved and the servo backlash errors and the apparent beam position error (Doviak and Zrnic', 1984) were comparable with the azimuthal displacement of the front. Such a problem is not present when the scans are in the same direction because the bias errors are canceled by the tracking procedure.

In Table 6 we summarize some of the parameters obtained from the algorithm. Comparing Table 6 with Tables 3 to 5 and Figs. 15, 16, 22, and 25 we conclude that the average shear is very similar to the average of maximum gradients, which is to be expected for fronts of similar intensity. The average flux is higher than the average momentum, by about a factor of 2 to 3, and the rms errors for this example are equal to the average value of the other cases.

4.5. April 26, 1984

Because the winds ahead of this front (Fig. 1) were very turbulent and disrupted flights from and to the Will Rogers Airport in Oklahoma City, we included this case in our tests. The frontal outflow was rather shallow (<1 km) and the discontinuity could be seen clearly only at 0.5° in

TABLE 6

Parameters for the April 10, 1981, Front*

TIME (CST)	CENTER r (km)	CENTER az (deg)	AVERAGE SHEAR ($m \cdot s^{-1} \cdot km^{-1}$)	AVERAGE MOMENTUM ($m \cdot s^{-1} \cdot km$)	LENGTH (km)	RMS ERROR (km)
2259	57	218	5.1	68	70	1.2
2300	55	218	4.6	64	70	1.2
2306	52	211	5.5	66	79	2.2
Average	55		5.0	63	73	1.5

*Elevation = 0.8°

elevation. At the next elevation, 1.5°, it was not visible. Of the detected shears at 2042 CST (Fig. 32a) No. 1 is the primary front and No. 2 a secondary surge; Nos. 3 and 4 are spurious shears that did not have time continuity. The shape of the primary front depicted by a five-point running average of maximum gradient location in Fig. 32a reproduces very well the pattern of Fig. 1a. The forecast position (Fig. 32b) agrees with the actual location of the front even though the forecast center and the actual center are displaced by about 10 km. Their displacement is along the frontal discontinuity and thus does not affect the front's position in range but only influences its azimuthal extent. Tabulated parameters (Table 7) are generally consistent with previous cases. The RMS error is on the high side because the front is long and has kinks; therefore, a second-order polynominal is not a best model for its shape.

5. Summary and Conclusions

The procedure we have developed to automatically detect and track gust fronts does not rely on a single method but requires simultaneous operation of several related algorithms. These algorithms process one or two radials of Doppler velocity data in real time. We have not incorporated in

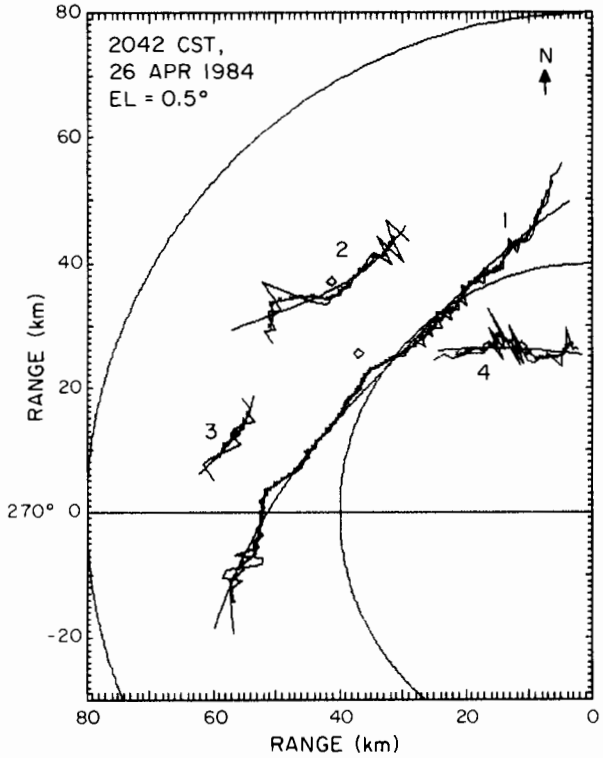

Figure 32(a) Shear lines detected by the gradient algorithm for April 26, 1984. The data, their five-point average, and the least square fitted curves are drawn.

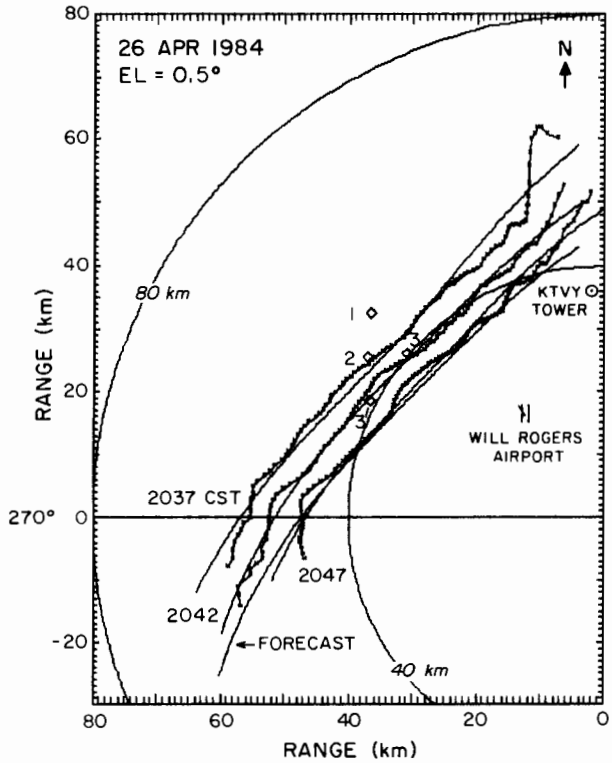

Figure 32(b) Three consecutive positions of the front. Five-point running average, least squares fitted curves, and a forecast position are shown. Square indicates the center of each curve.

TABLE 7

Parameters for the April 26, 1984, Front

TIME (CST)	ELEVATION ANGLE (deg)	RANGE OF CENTER (km)	HEIGHT OF CENTER (km)	AVERAGE OF MAX GRADIENT ($m \cdot s^{-1} \cdot km^{-1}$)	AVERAGE OF "FLUX" ($m \cdot s^{-1} \cdot km$)	LENGTH (km)	RMS ERROR (km)
2037	0.5	49	0.57	9.7	437	91	2.6
2042	0.5	45	0.51	9.0	361	80	1.6
2047	0.5	41	0.46	9.5	351	77	1.8
Average		45		9.4	383	85	2.0

our programs the simultaneous operations but have separately tested the various subsets of a general low level (less than 3 km above ground) hazard detection algorithm. The flow chart in Fig. 33 depicts the low level hazard algorithm as we envision it. In order to discriminate between gust fronts and short convergence lines, a convergence algorithm developed in this report is used. Calculations commensurate with radial update rates are required on one radial at a time for constructing pattern vectors that are later (at the end of a scan) sorted into features. Our convergence algorithm measures the radial convergence, and hence only gusts propagating along radials can be readily detected. For detecting gusts that are aligned along radials, we have employed the mesocyclone-shear algorithm, which requires storage and operation on two consecutive radials of velocity data. The long shear lines that this algorithm detects are classified as gusts whereas symmetric shear features are rejected if their shears and momentum are insignificant or are classified as low-level vortices that are known to accompany wavelike gusts. Shears of intermediate length (10 to 20 km) may be classified as spurious.

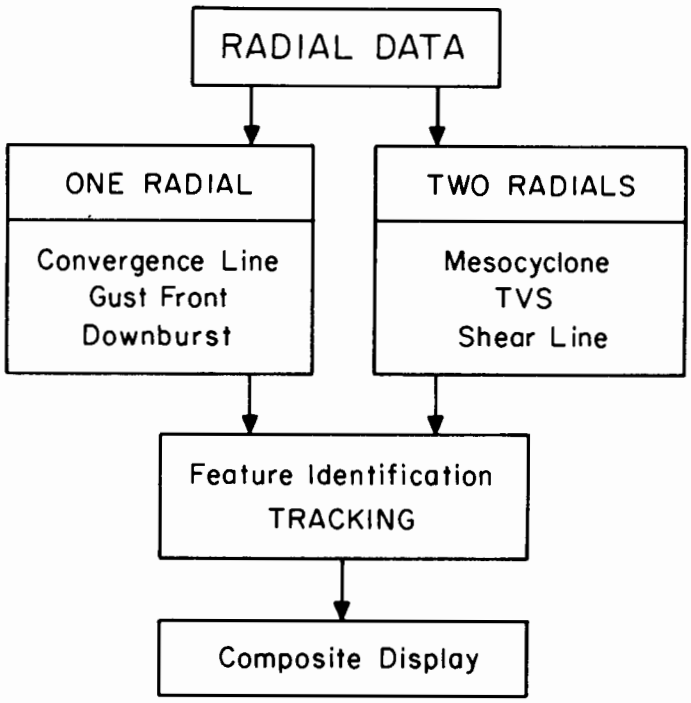

Figure 33 Algorithm for detecting weather hazards near the ground.

(Downdraft) and tornado vortex signatures (TVS) represent low level hazards that can be detected with the same basic technique of building pattern vectors, and that is why they are included in the flow chart (Fig. 33) even though they have not been developed yet. Other low-level hazards such as turbulence and hail require spectrum width and reflectivity data as well as different algorithms for identification; that is why they are not included in the chart.

After sorting of pattern vectors, the resulting features are classified and tracked. It appears that convergence lines (i.e., lines obtained from the convergence algorithm) shorter than 10-20 km can be discarded. Distinguishing by length and symmetry between hazardous and spurious features is not unique with the mesocyclone-shear algorithm because mesocyclones are symmetric and of small extent as are spurious shear lines. Therefore, checking the length and continuity in time may be a most effective means to eliminate spurious shears.

For tracking we used the center of gust lines and projected a second-order least squares curve fitted in range or azimuth. This simple procedure gave very satisfactory performance as can be seen from the summary of rms

errors in Table 8. About half the errors are produced by the statistical uncertainty in the locations of maximum gradients, and the other half are due to true deviations about the assumed second-order polynomial.

The distances between the radar and the centers of fronts ranged from 28 to 68 km, and the front's lengths were 25 to 85 km (Table 8). The variation in the average of maximum gradients is less than a factor of 2. Even less variation is evident in the average "flux". The low value of 63 $m \cdot s^{-1}$ km for April 10, 1981, is actually "momentum" obtained with the mesocyclone algorithm at constant ranges and along azimuths. At the ranges of observation, azimuthal smoothing by the beam extends over longer distances than the smoothing by the range weighting function and is therefore responsible for the lowest shear and momentum in Table 8.

Overall detection of gust fronts from measurements of radial velocity gradients and azimuthal shear is feasible. The results exceeded our expectations; there was no undetected front among the test cases. However, spurious shear and false alarms due to overlaid echoes were inevitably present. These can be significantly reduced by checking their length as well as time and height continuity.

TABLE 8

Average Parameters for Five Gust Fronts

DATE	RANGE OF CENTER (km)	AVERAGE OF MAX GRADIENT ($m \cdot s^{-1} \cdot km^{-1}$)	AVERAGE OF "FLUX" ($m \cdot s^{-1} \cdot km$)	LENGTH (km)	RMS ERROR (km)
April 13, 1981	28	5.9	255	30	1.3
May 9, 1981	68	5.2	231	48	2.1
May 29, 1981	34	9.1	335	25	0.6
April 10, 1981*	55	5.0	63	73	1.5
April 26, 1984	45	8.4	383	85	2.0
Average for five fronts	46	6.7	253	52	1.4

*This front was detected with the mesocylone-shear algorithm; the rest were detected with the convergence algorithm.

APPENDIX A

Measurement of mass flux with a Doppler radar

The air mass flux of a purely divergent flow can be estimated from measurements of radial velocities by a single Doppler radar. Consider a divergent symmetric flow in the azimuth range plane as on Figure A.1, and let the divergence extend over a depth larger than the angular extent (in elevation) of the resolution volume ($r\theta_1$); r is range to the divergence source and θ_1 antenna beamwidth. The air mass flux F_a through a cylinder of height $r\theta_1$ and diameter D is:

$$F_a = \pi D r \theta_1 \cdot v \cdot \rho \qquad (A.1)$$

where ρ is air density and v the magnitude of velocity at a distance D/2 from the source center. The radar with its beam centered on the divergence measures velocities v_b and v_e. Even if there is a uniform flow superposed on the divergent flow the difference $v_e - v_b = 2v$. Thus the radar estimated flux F_r is:

$$F_r = \pi(r_e - r_b)(r_b + r_e)(v_e - v_b)\theta_1 \rho/4 \qquad (A.2)$$

Because we have assumed that the depth of divergent flow is larger than $(r_b + r_e)\theta_1/2$ we normalize (A.2) with respect to this quantity:

$$2F_r/(r_b + r_e)\theta_1 = \pi(r_e - r_b)(v_e - v_b)\rho/2 \qquad (A.3)$$

Furthermore, $\pi\rho/2$ is a constant of no consequence in the algorithm so that $(r_e - r_b)(v_e - v_b)$ is the only term proportional to flux. It is important to bear in mind that this physical explanation is valid for a symmetric divergent flow.

Gust fronts are modeled as convergent lines so that the "flux" looses it's physical meaning. Nevertheless, it has proven useful in detecting these phenomena.

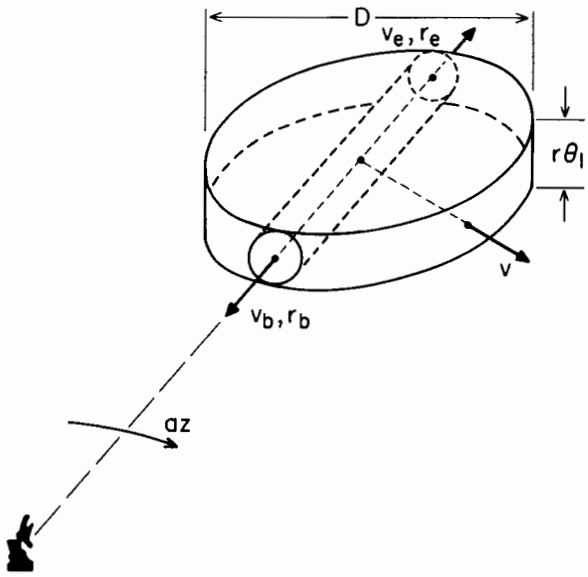

Figure A.1. Geometry of a mass flux measurement with a single Doppler radar for a purely divergent flow.

REFERENCES

Brown, R.A., L.R. Lemon, and D.W. Burgess, 1978: "Tornado detection by pulsed Doppler radar", **Mon. Wea. Rev., 106,** 29-38.

Doviak, R.J., and D.S. Zrnic', 1984: **Doppler Radar and Weather Observations.** Academic Press, New York, NY.

Goff, R.C., 1975: "Thunderstorm outflow kinematics and dynamics", **NOAA Tech. Memo ERL-NSSL-75.** Available from National Technical Information Service, Operations Div., Springfield, VA 22151.

Lemon, L.R., R.J. Donaldson, Jr., D.W. Burgess, and R.A. Brown, 1977: "Doppler radar application to severe thunderstorm study and potential real-time warning", **Bulletin, Am. Meteor. Soc., 58,** 1187-1193.

NEXRAD (Next Generation Weather Radar) Algorithm Report, 1984: Prepared by the NEXRAD Joint System Program Office.

Sirmans, D., and R.J. Doviak, 1973: "Pulsed-Doppler velocity isotach display of storm winds in real time", **J. Appl. Meteor., 12,** 694-697.

Wilson, J.W., R.D. Roberts, D. Kessinger, and J. McCarthy, 1984: "Microburst wind structure and evaluation of Doppler radar for airport wind shear detection", **J. Appl. Meteor., 23,** 898-915.

Wood, V.T., and R.A. Brown, 1983: "Single Doppler velocity signatures: An atlas of patterns in clear air/widespread precipitation and convective storms", **NOAA Tech. Memo. ERL NSSL-95.** Available from National Technical Information Service, Operations Div., Springfield, VA 22151.

Zrnic', D.S., and J.T. Lee, 1982: "Pulsed Doppler radar detects weather hazards to aviation", **J. Aircraft, 19,** 183-190.

Zrnic', D.S., and Y. Gal-Chen, 1983: "Divergence measurement in storm tops", Report for the Joint Systems Program Office.

Zrnic', D.S., and J.T. Lee, 1983: "Investigation of the detectability and lifetime of gust fronts and other weather hazards to aviation", FAA Report No. DOT/FAA/PM-83/33.

Zrnic', D.S., D.W. Burgess, and L.D. Hennington, 1984: "Automatic detection of mesocyclonic shear", accepted by the **J. Atmos. and Oceanic Technolgy.**